Doctoral Thesis in Electrical Engineering

# Multipoint measurements of solar wind magnetic holes

HENRIETTE TROLLVIK

KTH ROYAL INSTITUTE OF TECHNOLOGY

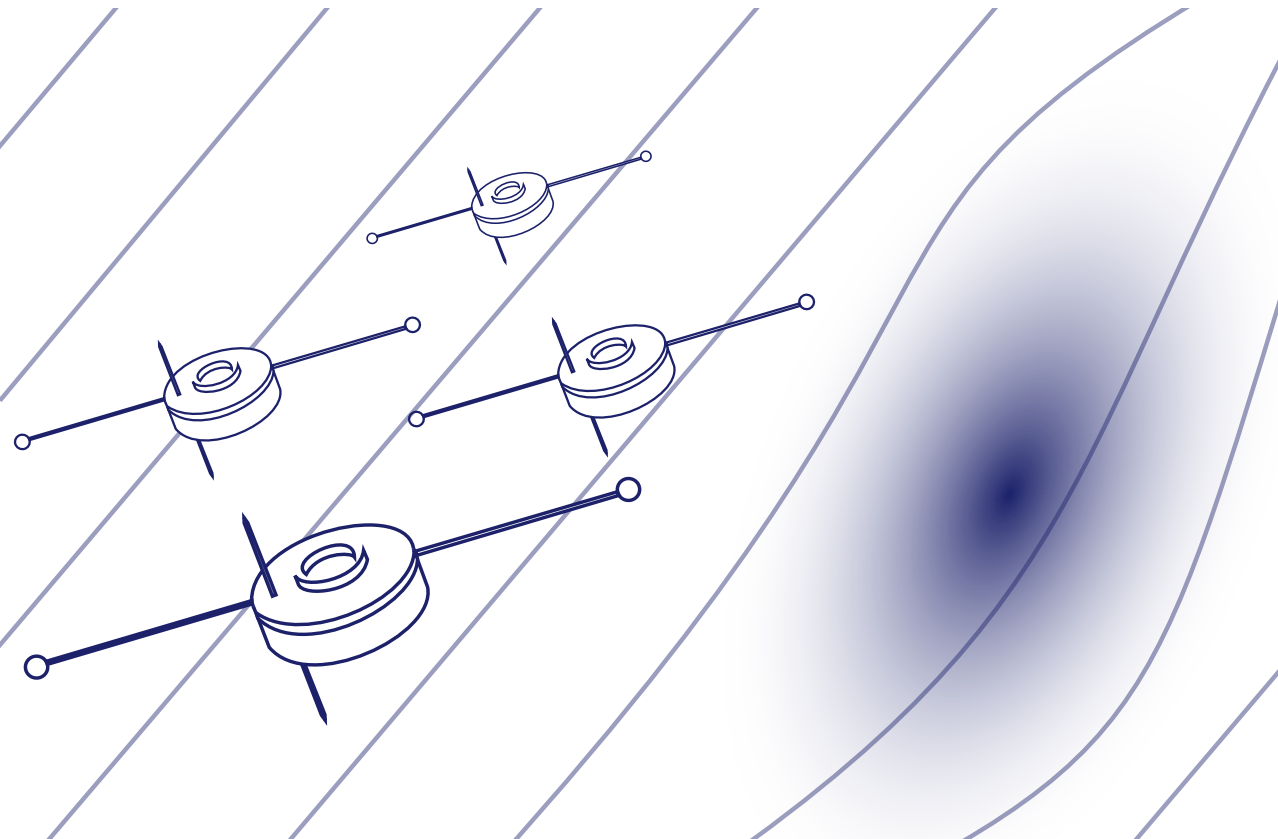

# Multipoint measurements of solar wind magnetic holes

HENRIETTE TROLLVIK

Academic Dissertation which, with due permission of the KTH Royal Institute of Technology, is submitted for public defence for the Degree of Doctor of Philosophy on Friday the 3rd of April 2025, at 1:00 p.m. in F3, Lindstedtvägen 26, Stockholm.

Doctoral Thesis in Electrical Engineering
KTH Royal Institute of Technology
Stockholm, Sweden 2025

© Henriette Trollvik

TRITA-EECS-AVL-2025:32
ISBN 978-91-8106-223-6

Printed by: Universitetsservice US-AB, Sweden 2025

**Abstract**

Magnetic holes (MH) are localized depressions of the magnetic field. They are found in various plasma environments, most commonly in the solar wind. The magnetic field direction sometimes varies across the hole, and it is common to divide MH into two categories, linear and rotational, where the first shows little to no rotation of the field. Linear MH are often in pressure balance with the surrounding plasma and can survive for long periods. It is unknown exactly where and how they are formed, but there is strong evidence that they are related to the mirror instability and waves associated with this instability. Rotational MH, on the other hand, appear as current sheet-like structures and are suggested to be related to magnetic reconnection or possibly in connection with wave activity. Both linear and rotational MH have similar properties, such as magnetic field magnitude and temporal scales.

In this thesis, we use the Cluster mission, which has four spacecraft moving closely together providing multipoint measurements, to understand the phenomenon of magnetic holes better. Cluster provides over 20 years of data, with varying spacecraft spacing. Sometimes, the spacing of the satellites is such that one satellite is located in the solar wind while another is in the magnetosheath. In these instances, we have identified the same MH in the solar wind and later in the magnetosheath, suggesting they can cross the bow shock (Paper I). Using the Cluster database, we have identified times when the same MH was observed with all four spacecraft. Applying a timing analysis on a subset of these, we have derived their velocity, and conclude that they are convected with the solar wind speed (Paper II). When the same MH is observed by all four satellites in the solar wind, based on the spacecraft separation, one has four measuring points separated by distances comparable to the size of the MH. These observations can be combined with a local coordinate transformation and a model to estimate the scales of the MH and derive information about the three-dimensional morphology of MH (Paper III). A large number of events were identified, and the results were combined to provide a statistical analysis of the morphology of solar wind magnetic holes (Paper IV).

**Keywords:** solar wind, plasma, magnetic holes, multipoint measurements, Cluster satellites

**Sammanfattning**

Magnetiska hål (MH) är lokaliserade reduktioner av magnetfältet. De finns i olika plasmamiljöer, oftast i solvinden. Det magnetiska fältets riktning varierar ibland över hålet, och det är vanligt att dela in MH i två kategorier, linjära och roterande, där den första visar liten eller ingen rotation av fältet. Linjära MH är ofta i tryckbalans med omgivande plasma och kan överleva under långa perioder. Det är okänt exakt var och hur de bildas, men det finns starka bevis för att de är relaterade till spegelinstabiliteten och vågor associerade med denna instabilitet. Roterande MH, åt andra sidan, uppträder som strömskikt-liknande strukturer och föreslås vara relaterade till magnetisk omkoppling eller möjligen till vågaktivitet. Både linjära och roterande MH har liknande egenskaper, såsom magnetfältets styrka och tidsskalor.

I den här avhandlingen använder vi Cluster-missionen, som har fyra satelliter som rör sig tätt tillsammans och ger flerpunktsmätningar, för att förstå fenomenet magnetiska hål bättre. Cluster tillhandahåller över 20 års data, med varierande avstånd mellan satelliterna. Ibland är avståndet mellan satelliterna sådan att den ena satelliten befinner sig i solvinden medan en andra är i magnetoskiktet. I dessa fall har vi identifierat samma MH i solvinden och senare i magnetoskiktet, vilket tyder på att de kan korsa bogchocken (Paper I). Med hjälp av Cluster-databasen har vi identifierat tillfällen då samma MH observerades med alla fyra satelliter. Genom att tillämpa en tidsanalys på en delmängd av dessa har vi härlett deras hastighet och drar slutsatsen att de konvekteras med solvindens hastighet (Paper II). När samma MH observeras av alla fyra satelliterna i solvinden, baserat på rymdfarkostens separation, har man fyra mätpunkter åtskilda av avstånd jämförbara med storleken på MH. Dessa observationer kan kombineras med en lokal koordinattransformation och en modell för att uppskatta skalstorlekarnlorna för MH och härleda information om MH tredimensionella morfologi (Paper III). Ett stort antal händelser identifierades, och resultaten kombinerades för att ge en statistisk analys av morfologin för solvindens magnetiska hål (Paper IV).

# List of Papers

I *Solar wind magnetic holes can cross the bow shock and enter the magnetosheath*
Karlsson, T., **Trollvik, H.**, Raptis, S., Nilsson, H., and Madanian, H.
*Annales Geophysicae (2022)*

II *Velocity of magnetic holes in the solar wind from Cluster multipoint measurements*
**Trollvik, H.**, Karlsson, T. and Raptis, S.
*Annales Geophysicae (2023)*

III *Morphology of magnetic holes: Methodology and case studies*
**Trollvik, H.**, Karlsson, T. and Raptis, S.
*Journal of Geophysical Research - under review*

IV *Statistical analysis of the morphology of magnetic holes in the solar wind close to 1 AU*
**Trollvik, H.**, Karlsson, T., Bergman, S. and Wong Chan, T. K.
*Journal of Geophysical Research - submitted*

Other contributions by the author not included in the thesis.

- *Classifying the magnetosheath behind the quasiparallel and quasi-perpendicular bow shock by local measurements*
  Karlsson, T., Raptis, S., **Trollvik, H.**, and Nilsson H.,
  *Journal of Geophysical Research: Space Physics (2021)*

- *On magnetosheath jet kinetic structure and plasma properties*
  Raptis, S., Karlsson, T., Vaivads, A., Lindberg, M., Johlander, A., and **Trollvik, H.**
  *Geophysical Research Letters (2022)*

- *Downstream high-speed plasma jet generation as a direct consequence of shock reformation*
  Raptis, S., Karlsson, T., Vaivads, A., Pollock, C., Plaschke, F., Johlander, A., **Trollvik, H.**, and Lindqvist, P.-A.,
  *Nature communications (2022)*

- *Simulations of the collection of mesospheric dust particles with a rocket instrument*
  Pineau, A., **Trollvik, H.**, Greaker, H., Olsen, S., Eilertsen, Y., and Mann, I.
  *Atmospheric Measurement Techniques (2024)*

- *Statistical properties of Short Large-Amplitude Magnetic Structures (SLAMS) in the foreshock of Earth from Cluster measurements*
  Bergman, S., Karlsson, T., T. K. Wong Chan. and **Trollvik, H.**
  *Journal of Geophysical Research: Space Physics - Under review*

# Acknowledgement

These years as a PhD student have been a tremendous learning experience, and while there have been challenges along the way, I am filled with gratitude and joy as this chapter comes to a close. This would not have been possible without the unwavering support of so many, and I am deeply thankful to all those who have been part of this journey.

First of all, I would like to thank my supervisor Tomas Karlsson, for all the scientific discussions. For teaching me what it means to be a good scientist. I am deeply grateful for your patience, constructive feedback, and belief in my work.

I would like to extend my sincere thanks to Martin Volwerk and the whole ISSI team on "Towards a Unifying Model for Magnetic Depressions in Space Plasmas" for including me in the magnetic holes network and for the interesting discussions and talks during our meetings.

A special thank you to my colleagues and friends that I have met over the years at KTH. To Savvas, for being very helpful with all questions, big or small, and to Sofia for all the support and help in the final months. Thank you to the rest of the SPP PhD students and postdoc: Sabrina, Konstantinos, Sushen, Judit, Maria, Fotios, Tsz, Tommaso, Chao, Anatol, and Rehab for fun AWs, fikas, meetings and more. I would also like to thank Ladislas, Federico, Emil, and Francesca for always being up for adventures, dinners, and rants over small and big problems. Thank you to Luca for reviewing the thesis, and to the remainder of the SPP staff for interesting conversations, meetings, and discussions. To Björn and Pilar, thank you for endless hours of pep and support. And to the rest of the PhD students at Teknikringen 31 for the fun times, interesting lunch talk, and fikas. I also want to thank the PhD students at IRF-Uppsala for our joint experiences with courses and harsh climates.

I would also like to acknowledge my friends back in Norway for all the phone calls, fun visits, and walks down memory lane. A special thank you to Kassi for all the study dates and for always taking the time to listen and help, science-related or not.

I want to thank my family, my parents, Annfrid and Asle, and my siblings, Karoline, Marte, and Aksel, for always being there supporting me and having given me the tools to handle what comes my way. And thank you to my Swedish family Lena and Janne, and the rest, for including so warmly to your family.

And finally, to my love, Tobias, who has been there through the good times and the bad, having you by my side made it all easier.

# Contents

**List of Papers** **iii**

**Acknowledgement** **v**

**Contents** **1**

**1 Introduction** **3**

**2 Near-Earth space and its physics** **7**
2.1 Definition of a plasma . . . . . 7
2.2 Single particle motion . . . . . 8
2.3 Plasma equations . . . . . 10
2.4 The solar wind . . . . . 14
2.5 Solar-terrestrial environment . . . . . 14

**3 Spacecraft missions** **17**
3.1 The Cluster mission . . . . . 17

**4 Spacecraft data analysis methods** **21**
4.1 Rankine-Hugoniot conditions . . . . . 21
4.2 Minimum variance analysis . . . . . 22
4.3 Timing analysis . . . . . 23

**5 Magnetic holes** **27**
5.1 Definition . . . . . 27
5.2 Linear magnetic holes . . . . . 28
5.3 Formation and origin . . . . . 31
5.4 Plasma properties of linear MH . . . . . 37
5.5 Rotational magnetic holes . . . . . 39

**6 Summary of the included papers** **41**
6.1 Paper I - Solar wind magnetic holes can cross the bow shock and enter the magnetosheath . . . . . 41

6.2 Paper II - Velocity of magnetic holes in the solar wind from Cluster multipoint measurements . . . . . 43
6.3 Paper III - Morphology of magnetic holes: Methodology and case studies . . . . . 45
6.4 Paper IV - Statistical analysis of the morphology of magnetic holes in the solar wind close to 1 AU . . . . . 47

**7 Discussion and outlook** **49**
7.1 Origin of magnetosheath MH . . . . . 49
7.2 Velocity of solar wind magnetic holes . . . . . 50
7.3 Morphology of magnetic holes in the solar wind . . . . . 50
7.4 Outlook . . . . . 51

**References** **53**

# Chapter 1

# Introduction

Many have spent some time looking up at the sky. You might have had the pleasure of seeing the northern lights dancing across the sky, enveloping you in bright light shifting in nuances of green, purple, and red. Or staring at the night sky and seeing some of the thousands of stars scattered across the sky. The distances are so big that the time it takes for the light to reach our eyes is longer than the lifetime of some of the stars themselves. It is easy to feel small once you start learning about the scales and vastness of the universe. In this thesis, we will stay close to Earth and not move too far out. The curiosity of looking up at the sky has driven scientists for generations to seek answers and develop new technology to do so. The advances in space technology have made space more accessible, and we can now do direct investigations of the near-Earth space environment and the solar system. Satellites have been used to study space, both directly with in-situ instruments like magnetometers measuring the local magnetic field, and remotely with telescopes and radars probing down to the surfaces of moons and planets. Space provides the perfect laboratory to study complex physics that would be difficult to recreate on Earth. And it all starts with the sun.

The sun is fueling the entire solar system with energy. Without it, the solar system would be cold and, as a matter of fact, not exist. There would be nothing holding all the planets and asteroids together in their orbits. Some of the energetic particles in the solar atmosphere escape the gravitation and are accelerated outwards to supersonic speeds. This continuous stream of charged particles is called the solar wind (SW). The solar wind is in a state of matter called the plasma state. It is a state where the temperature is so high that electrons are separated from the ions creating an electrically conducting gas. The existence of the solar wind was first hypothesized based on the shape and direction of the tail of comets (Biermann, 1951). The velocity varies depending on the details of the origin, with a mean velocity of 400 km/s (Kivelson and Russell, 1995). This supersonic flow of plasma will interact with the planets. What this interaction

looks like will depend on, among other things, the magnetic properties of the objects it encounters.

On Earth, we are lucky. The liquid interior provides us with a dipole magnetic field, essentially acting like a shield to this wind and its highly energetic particles. This is a very simple way of putting it, we will discuss it in more detail later in this thesis, but for the sake of this introduction, let's start simple. Even without the field, an object in a supersonic flow will result in a shock front. This is a boundary between the supersonic and the subsonic flow as a result of the influence of the obstacle. Shock dynamics is, again, complicated, but imagine a ship moving in calm water. At the front (called the 'bow'), a wave is created as the boat disturbs the water. For boats, this is called a bow wave, while in space, the equivalent is called the bow shock. In physics, motion can be described in different reference frames. In the boat analogy, the boat was moving. In space, it is the solar wind that passes the planet, but the picture is very similar. The bow shock marks where the solar wind is decelerated to interact with the planet, or in this case, due to the magnetic properties of the solar wind, the dipole field of the Earth. After passing the bow shock, the solar wind is quickly decelerated, and as a consequence, the plasma becomes heated, compressed, and more turbulent. This region is called the magnetosheath. The boundary between the interplanetary magnetic field and Earth's magnetic environment is called the magnetopause.

In this thesis, we stay outside of Earth's magnetic environment. The solar wind exhibits a range of plasma phenomena, from discontinuities to waves and turbulence. One phenomenon often observed in the solar wind and magnetosheaths is magnetic holes (MH). The first reported observations were made in the 1970s, and since then, there have been several observations at a range of distances from the sun. A magnetic hole is a localized region with a deep magnetic depletion, sometimes even a down to zero field strength. They are also often observed to be in pressure balance, where the density or temperature increases to compensate for the decrease in magnetic field. Most studies conducted have been made with single spacecraft missions. In this thesis the work has been focused on studying magnetic holes using multispacecraft measurements. The mission used is the ESA Cluster mission, which consisted of four spacecraft moving together in a tetrahedral configuration, most of the time. Over the years the distance between the spacecraft has been varied to allow studies of different scales. In this work this has been utilized to try to gain deeper insights into the phenomena of magnetic holes.

The work can be summarized into three main objectives:

1. Investigate the origin of magnetosheath magnetic holes

2. Determine the velocity of solar wind magnetic holes

3. Investigate the morphology of magnetic holes in the solar wind

The thesis is organized as follows: Chapter 2 serves as a background and introduction to central space plasma physics phenomena and the different plasma environments considered in this work. In Chapter 3 the Cluster mission and the relevant instruments are presented. Chapter 4 introduces some analysis techniques. Chapter 5 contains a short summary of some of the magnetic hole research and theories. Chapter 6 contains the summary of the papers included in the thesis and Chapter 7 is a discussion and outlook.

# Chapter 2

# Near-Earth space and its physics

Before introducing the concept of the space environment and, in the end, magnetic holes, we first need to understand the plasma state of the matter.

## 2.1 Definition of a plasma

In Chen and others (1984), a plasma is defined as: *"(...) a quasineutral gas of charged and neutral particles which exhibits collective behavior"*.

It is often referred to as a "fourth state of matter", where the gas is so hot that it becomes ionized, meaning that the atoms are split into electrons (e) and ions (i). In order for an ionized gas to be considered a plasma, certain conditions should be met.

The ionized nature of the plasma means it is strongly affected by electric and magnetic fields. A charged particle introduced into the plasma will result in an electric field. However, the charges in the plasma will redistribute and be attracted or repulsed depending on their charge. This will shield the electric field from the rest of the plasma. The effective size of the shielding region is characterized by the Debye length, given by

$$\lambda_D = \sqrt{\frac{\epsilon_0 k_B T_e}{n e^2}} \tag{2.1}$$

where $\epsilon_0$ is the vacuum permitivity, $k_B$ is the Boltzmann constant, $T_e$ is the electron temperature, $n$ is the plasma number density and $e$ is the unit charge. In the plasma considered in this thesis, the Debye length is determined by the electrons, as they have a much higher temperature than the ions. The shielding of the plasma results in its quasi-neutrality, and the number density of the ions and electrons are approximately the same, under the condition that the characteristic length scale of the plasma is much larger than the Debye length. In the solar wind, the Debye length is approximately 10 m, and the characteristic length is larger than the gyro radius (see Section 2.2), which is on the order of 100 meters

for electrons and on the order of 100 kilometers for ions. In addition, there needs to be enough particles for the shielding to be efficient.

The Debye length is closely related to the plasma frequency $\omega_p$. The response from the plasma particles to redistribute and shield the electric field results in an oscillation of the plasma. This motion is called plasma oscillation and has an (angular) frequency (called the 'plasma frequency'), given as

$$\omega_{p,s} = \sqrt{\frac{ne^2}{\epsilon_0 m_s}} = \frac{1}{\lambda_D}\frac{k_B T}{m_s} \tag{2.2}$$

Here, $s$ refers to the species (i for ions and e for electrons). This means that if the plasma frequency is high, the Debye length is short, and the plasma responds quickly to an external electric field.

Temperature is an important parameter in plasmas. It is closely related to the average kinetic energy of the particles in the plasma and is thus often given in terms of electronvolts (eV), where 1 eV $= 1.6 \cdot 10^{-19}$ J. Temperature also reflects the spread of the velocity of the individual particles, i.e the velocity distribution. In a plasma, the individual species can have different temperatures. Sometimes, even the same species can have different temperatures with respect to the magnetic field direction. The thermal velocity is the average velocity of particles due to their thermal energy, and can be expressed in terms of species as

$$v_{th,s} = \left(\frac{k_B T}{m_s}\right)^{1/2} \tag{2.3}$$

Another important plasma parameter is the plasma beta ($\beta$), which is the ratio of the plasma thermal pressure to the magnetic pressure;

$$\beta = \frac{p}{B^2/\mu_0} = \frac{nk_b T}{B^2/\mu_0} \tag{2.4}$$

where B is the magnetic field magnitude, p is the thermal pressure, and $\mu_0$ is the vacuum permittivity. For a high $\beta$ plasma, the thermal pressure dominates over the magnetic pressure, which is often the case in space. For low $\beta$, the magnetic pressure dominates, which is often the case close to Earth, where the geomagnetic field is strong.

## 2.2 Single particle motion

The basic motion in a plasma is that of the single charged particles. In the presence of magnetic and electric fields, the force acting on a particle is called the Lorentz force and is given by

$$F = q(\mathbf{E} + \mathbf{v} \times \mathbf{B}) \tag{2.5}$$

where $q$ is the charge of the particle and $\mathbf{v}$ is its velocity. The force due to the electric field ($\mathbf{E}$) is along the electric field itself, while the force due to the magnetic field ($\mathbf{B}$) depends on the velocity of the particle. When a charged particle is subjected to electromagnetic fields, the force acting on the particle will result in a change in motion. For a charged particle in the solar wind or in the Earth's magnetosphere, this results in three main types of motion: (1) gyration, (2) drift, and (3) bouncing. When the only force acting on the particle is a constant magnetic field, the particle will gyrate with a gyro (or cyclotron) frequency. Since the magnetic force depends on charge, ions and electrons will gyrate in opposite directions. The gyration is illustrated in Figure 2.1a. Here, the guiding center is the center of the gyration of the particles. The circular motion of the particles results in a current in the direction of the gyrating particles (same direction of ions, opposite direction of electrons). The magnetic field induced by this current opposes the external magnetic field, a phenomenon known as the *diamagnetic effect*. This is a central effect in the formation theories of magnetic holes.

The radius of the gyration is called the gyro (or cyclotron or Larmor) radius, expressed as

$$\rho_s = \frac{m_s v_{s,\perp}}{|q_s| B} \tag{2.6}$$

where $s$ denotes the species, $q$ is the charge and $v_\perp$ is the perpendicular velocity. When we talk about parallel and perpendicular components, this refers to the background magnetic field. The gyro radius is often a good measure of the plasma scale of a structure, and in regards to magnetic holes, the ion gyro radius is often used as a unit of the MH size.

This simple gyration is modified in the presence of electric fields and non-uniform, time-varying magnetic fields, leading to a drift motion. There are several types of drifts, the most common ones being the E $\times$ B drift, caused by the presence of an electric field, and the gradient drift, caused by the presence of a spatial gradient of the magnetic field. A general expression for the drift of a particle due to a force ($\mathbf{F}$) acting on a particle can be given as

$$\mathbf{v_F} = \frac{1}{q} \frac{\mathbf{F} \times \mathbf{B}}{|B|^2} \tag{2.7}$$

and hence the E $\times$ B drift is

$$\mathbf{v_{E \times B}} = \frac{\mathbf{E} \times \mathbf{B}}{|B|^2} \tag{2.8}$$

It is only the perpendicular component of the force that results in drift motion. Figures 2.1b and 2.1c illustrate the drift of ions and electrons in the presence of an electric field and a magnetic field spatial gradient, respectively. The E $\times$ B drift is independent of charge, and hence ions and electrons drift in the same direction, as compared to the gradient drift.

The third type of particle motion is bouncing. This is the result of the gyro motion mentioned earlier, in combination with one of the adiabatic invariants, namely the conservation of the magnetic moment of a charged particle. This is given as

$$\mu = \frac{mv^2 \sin^2(\alpha)}{2B} \tag{2.9}$$

where $\alpha$ is the pitch angle, which is the angle between the velocity and the magnetic field. For $\alpha = 0°$, the particle is moving parallel to the magnetic field, while for $\alpha = 90°$, the particle is moving perpendicular to it. If the magnetic field changes slowly compared to the gyro frequency of the particle, which is always the case for the space plasma considered in this thesis, $\mu$ is conserved. If we now consider a magnetic field that converges, meaning the spatial gradient is non-zero, on two sides, and expands in the middle, like Figure 2.1, due to the conservation of the magnetic moment of the particle, particles with certain pitch angles will be trapped. This is because the increase in the field needs to be balanced by a change in the pitch angle, to keep the magnetic moment and particle energy constant. At a certain point, the parallel velocity will be zero, and the particle will be reflected. The critical pitch angle of trapped particles is defined as $\alpha_c = \sin^{-1}[(B_{min}/B_{max})^{1/2}]$, where $B_{min}$ and $B_{max}$ is the magnetic field strength at the weakest and strongest (mirror) point. This trapping results in bouncing between regions of converging field lines, as is the case of the magnetic field of the Earth, where the field lines converge at the poles. This bouncing motion is illustrated in Figure 2.1d. In magnetic holes, which is the main topic of this thesis, this bounce motion is believed to play a role in the formation of the holes, and is central to the mirror instability, which we will come back to later in Chapter 5.

The plasma can also be described in more complex ways, by taking into account the interaction between particles and fields; these are the fluid and kinetic descriptions.

## 2.3 Plasma equations

### Electromagnetic equations

The particle density in interplanetary plasma is often low, and thus, traditional binary collisions rarely happen. The interaction between the particles is, on the other hand, dominated by long-range electromagnetic forces. The fundamental equations in all electromagnetic theory are the Maxwell equations. They explain how the fields (electric and magnetic) are connected to each other and to the plasma (or other mediums). The fact that the plasma contains charged particles means that electric and magnetic fields will be induced and affect the plasma. Maxwell's equations are given as

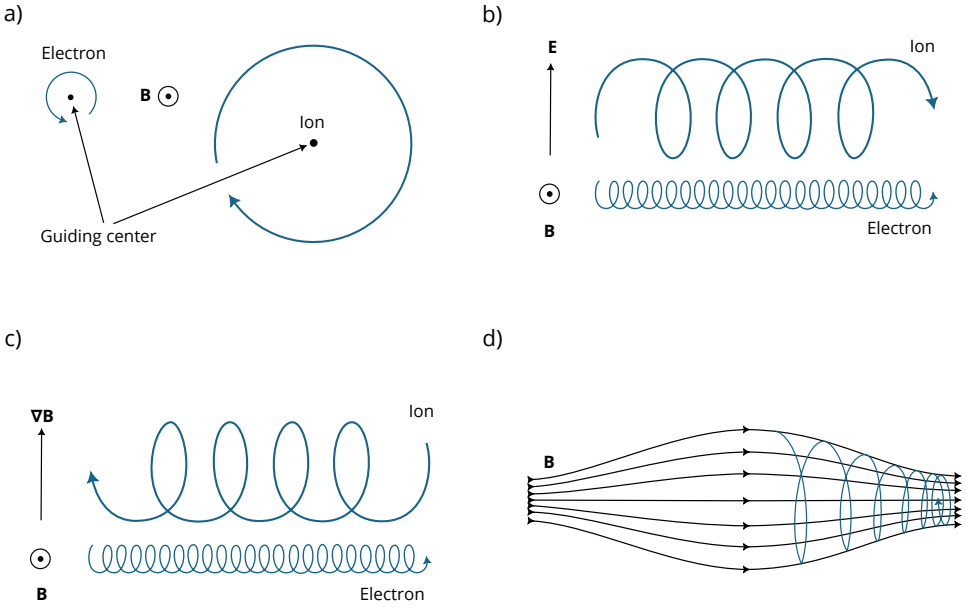


Figure 2.1: Illustration of particle motion in the presence of various fields. Adapted from (Baumjohann and Treumann, 2012)

$$\text{No magnetic monopoles:} \quad \nabla \cdot \mathbf{B} = 0 \tag{2.10}$$

$$\text{Gauss' law:} \quad \nabla \cdot \mathbf{E} = \rho/\varepsilon_0 \tag{2.11}$$

$$\text{Ampere's law:} \quad \nabla \times \mathbf{B} = \mu_0(\mathbf{J} + \varepsilon_0 \frac{\partial \mathbf{E}}{\partial t}) \tag{2.12}$$

$$\text{Faraday's law:} \quad \nabla \times \mathbf{E} = -\frac{\partial \mathbf{B}}{\partial t} \tag{2.13}$$

Here $\rho$ is the charge density, $\mathbf{J}$ is the current density, and $\varepsilon_0$ and $\mu_0$ are the permittivity and permeability of free space. Equation 2.10 states that magnetic monopoles cannot exist, meaning that magnetic field lines are always continuous closed loops. Equation 2.11, Gauss' law, describes how field lines are connected from a positive charge to a negative charge. Equation 2.12, Ampere's law, relates how the magnetic field changes with the current and a time-varying electric field. Equation 2.13, Faraday's law, relates how the electric field changes with a time-varying magnetic field.

The electrical properties of the plasma can often be described by Ohm's law, which in its general form states

$$\mathbf{E} + \mathbf{v} \times \mathbf{B} = \eta \mathbf{J} + \frac{1}{en}(\mathbf{J} \times \mathbf{B} - \nabla \cdot \mathbf{P}) \tag{2.14}$$

where $\eta = 1/\mu_0\sigma$ is the magnetic diffusivity, where $\sigma$ is the conductivity. $\mathbf{P}$ is the pressure tensor, accounting for thermal pressure and anisotropies in the plasma. Equations 2.10-2.14 are the basic equations to describe the electromagnetic properties of a conducting fluid.

## Fluid equations

There are two main ways of describing the plasma: either one considers the individual motion of the particles (kinetic approach), or one considers the plasma as a fluid (fluid approach, often magnetohydrodynamics (MHD)). Which method to use depends on the length scale of the plasma in question and what plasma phenomenon one wants to study. For simulations, a full kinetic treatment is difficult, and thus, a combination of the fluid and kinetic approach is often used.

In the fluid description, plasma is considered a continuous medium, whereas single-particle motions are not considered. Maxwell's equations are the first set of equations, but we need three more to complete the set. The first is the momentum equation;

$$m_s n_s [\frac{\partial \mathbf{v}_s}{\partial t} + (\mathbf{v}_s \cdot \nabla)\mathbf{v}_s] = q_s n_s (\mathbf{E} + \mathbf{v}_s \times \mathbf{B}) - \nabla p_s \tag{2.15}$$

where $s$, again, denotes the particle species, i.e. ion species or electrons. This equation tells us how the plasma responds to the fields consistent with the conservation of momentum. The next equation is the continuity equation;

$$\frac{\partial n_s}{\partial t} + \nabla \cdot (n_s \mathbf{v_s}) = 0 \tag{2.16}$$

which describes the conservation of matter, meaning that the total number of particles is conserved. The final equation we need is one relating the pressure to known quantities. Two methods are commonly used, either through isothermal closure; $p_j = n_j k T_j$ or for fast time variations; $T = T_0(\frac{n_j}{n_0})^{\gamma-1}$, $p = p_0(\frac{n}{n_0})^{\gamma}$, $\gamma = (d+2)/d$. Here $d$ is the number of degrees of freedom. This closes the set of equations, and there are equal numbers unknowns and equations.

The solar wind can often be described by the so-called ideal MHD model/equations. In this model, the plasma as a whole is treated as one electrically conductive fluid and is valid for scales much larger than the characteristic length scale of the plasma. The plasma is considered as a single species fluid, which means that the current and density can now be considered as a sum over all particle species instead $J = \sum_s q_s n_s v_s$ and $\rho = \sum_s q_s n_s$. In the fluid equations above, $n_j$ and $v_j$ are simply $n$ and $v$ as the fluid moves as one. In addition, the Ohm's law (Equation 2.14) in ideal MHD where the conductivity is assumed to be infinite, takes the form;

$$\mathbf{E} + \mathbf{v} \times \mathbf{B} = 0 \tag{2.17}$$

A result of the MHD approach is the 'frozen-in' phenomenon. It states that plasma and magnetic field lines move together, and is the result of the high conductivity. Whether the magnetic field is frozen into the plasma or not can be quantified by the magnetic Reynolds number $R_m$, which is the estimated ratio of the magnetic induction and diffusion. For high values, like in the solar wind, the conductivity is very high, and magnetic diffusion is neglected. In other words, the magnetic Reynolds number can act as a measure of whether the MHD model can be applied to the problem or not.

A perturbation of the plasma results in oscillations, waves, or instabilities. One of the most common MHD waves is the Alfvén wave, which propagates parallel to the magnetic field. The propagation velocity is given by

$$v_A = B/\sqrt{\mu_0 \rho_m} \tag{2.18}$$

where $\mu_0$ is the permeability of vacuum and $\rho_m$ is the mass density. Alfvén waves are central in space plasmas, and some formation mechanisms of MH involve the Alfvén wave.

The fluid approximation is often sufficient, but when investigating instabilities, such as the mirror instability, a kinetic description is often needed.

### Kinetic equations

In the kinetic picture, the distribution of the particle species are given as $f_e(\mathbf{x}, \mathbf{v}, t)$ and $f_i(\mathbf{x}, \mathbf{v}, t)$, which for the fluid approach was assumed to be Maxwellian and only dependent on temperature. If we consider a collisionless plasma (e.g. the solar wind), the plasma is hot enough for collisions to be neglected, and the only force acting on the particles is the Lorentz force (2.5), then the change in the plasma can be described by the Vlasov equation;

$$\underset{(1)}{\frac{\partial f_s}{\partial t}} + \underset{(2)}{\mathbf{v_s} \cdot \nabla_{\mathbf{x}} f_s} + \underset{(3)}{\frac{q}{m}(\mathbf{E} + \mathbf{v_s} \times \mathbf{B}) \cdot \nabla_{\mathbf{v}} f_s} = 0 \tag{2.19}$$

The Vlasov equations describe the total time derivative of the distribution function via the chain rule. The first term is the implicit time variation of the distribution. The second term is due to the change in position, and the third is due to the change in velocity associated with the force acting on the particle. With a kinetic approach using the distribution function of the species, the density and current are the zeroth- and first-order moments of the distribution function, $\rho = \int q f dv^3$ and $\mathbf{J} = \int q \mathbf{v} f dv^3$. The second-order moment is the pressure, which is related to the temperature through the ideal gas law $p = k_B n T$, which holds in solar wind conditions.

## 2.4 The solar wind

The framework to study space plasmas is introduced above. With that in mind, the different regions of space considered in this thesis can be introduced.

In addition to radiation, the sun continuously emits a stream of (fully ionized) plasma called the solar wind. The solar wind is the result of the expansion of the solar corona. It flows radially outward from the sun where, as explained earlier, the magnetic field is frozen in and dragged outwards with it. The radial motion of the plasma, combined with the rotation of the sun, results in the magnetic field lines being bent in a spiral shape, similar to the shape of the water coming out of a rotating water sprinkler. The solar wind magnetic field is often referred to as the interplanetary magnetic field (IMF).

The solar wind consists mostly of electrons and protons and a small fraction of heavier ions. The speed ranges between 300 and 1200 km/s depending on the conditions of the origin in the solar corona and surface. The slow solar wind is thought to typically originate in the equatorial plane of the sun, while the fast wind originates from the polar region. Average solar wind parameters close to the Earth are; density $n_e \approx 5$ cm$^{-3}$, temperature $T_e \approx 10^5$ K and the interplanetary magnetic field (IMF) is on the order of 5 nT. The solar wind is often characterized by a narrow cold particle distribution and is easily identified in spacecraft measurements by the narrow energy spectrum.

The solar wind is supersonic and super-Alfvénic. In ordinary air, the characteristic speed is the speed of sound. However, in space plasmas, the dynamics are governed by the motion of charged particles, and the relevant wave speed is the Alfvén speed. When the solar wind is super-Alfvénic, it travels faster than Alfvén waves, preventing these waves from propagating upstream. This has significant implications for wave-particle interactions and the behavior of the solar wind as it moves away from the Sun. One implication is shocks, which will be addressed in the next section. As the solar wind moves outwards, it will interact with the planets and other solar system objects. The interaction will vary depending on the magnetic properties of the solar system object that the solar wind encounters. In this thesis, we only focus on the Earth, which, due to its liquid core and rotation, has a strong dipole magnetic field.

## 2.5 Solar-terrestrial environment

Earth's magnetic field acts as a shield for the solar wind and results in a complex environment, which in turn interacts with the solar wind in a range of ways. The solar-terrestrial environment is commonly divided into several regions and boundaries separating different plasma regions. These regions are illustrated in Figure 2.2.

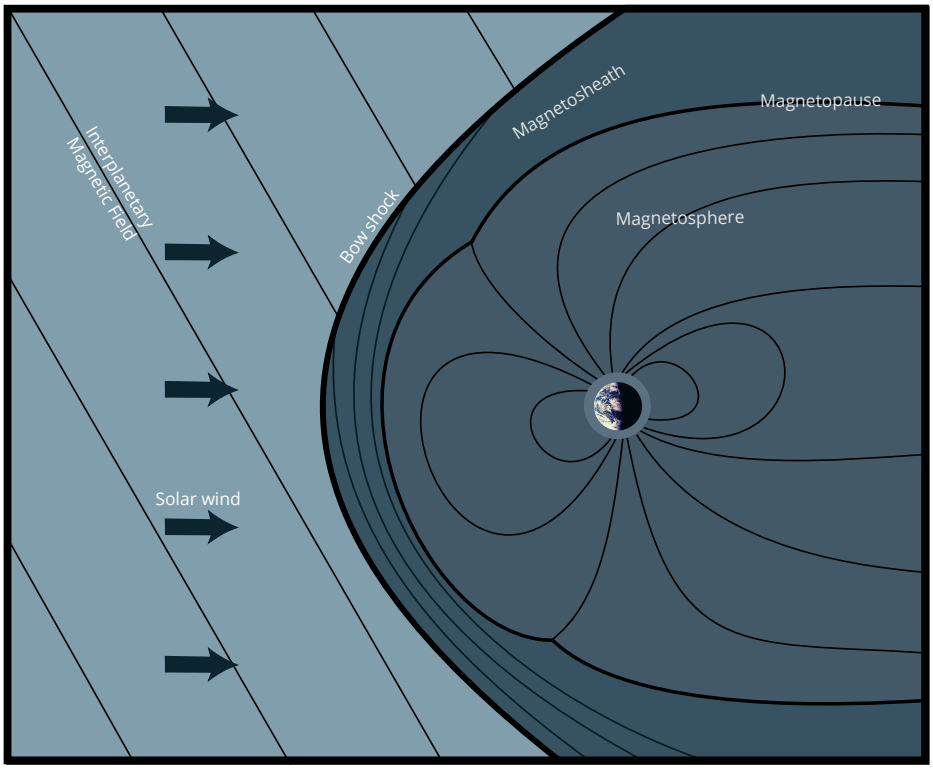


Figure 2.2: Solar-terrestrial environment. Adapted from (Baumjohann and Treumann, 2012)

### Bow shock

As mentioned, the bow shock is the boundary where the solar wind is abruptly slowed down, and the kinetic energy of the plasma is converted to thermal and magnetic energy. Earth's bow shock and most shocks in space are collisionless due to the low density, and thus, the shock is the result of the long-distance interactions mediated by electromagnetic fields. When talking about the bow shock and the regions close to it, the nomenclature is to refer to the part in the solar wind side of the shock as *upstream*, and the region on the other side of the shock as *downstream*.

The bow shock is often divided into two regions, called the *quasi-parallel* and *quasi-perpendicular* shock. In the *quasi-parallel* region, where the angle between the IMF and the bow shock normal is close to zero, the solar wind ions reflected at the bow shock can travel far upstream, resulting in a turbulent region and wave generation called the *foreshock* (Burgess et al., 2005). This region has similar

properties to the solar wind, but the temperature of the ions increases, resulting in a broadened particle distribution. In spacecraft observations, this is often identified by the particle energy spectrum.

In the other case, *quasi-perpendicular*, the direction of the IMF is close to perpendicular to the bow shock normal. Here, there is less interaction between the solar wind beam and reflected ions, resulting in a calmer environment both upstream and downstream of the shock.

### Magnetosheath

After the solar wind has crossed the bow shock, it is decelerated to subsonic velocities and thermalized. As a result, the temperature and density increase. The deceleration of the flow also leads to a compression of the magnetic field since it is frozen into the plasma flow. This region is called the magnetosheath. The magnetosheath behind a quasi-parallel shock is often much more turbulent than that behind the quasi-perpendicular shock. The magnetosheath exhibits a range of instabilities, among others the mirror instability, which will be discussed more in Chapter 5. This instability is the result of temperature anisotropy, which behind a quasi-perpendicular shock is caused by perpendicular heating due to the shocked solar wind, with an additional field-aligned outflow resulting in parallel cooling of the plasma in the dayside (Treumann and Baumjohann, 1997).

### Magnetosphere

The boundary between the space plasma and the magnetosphere is called the *magnetopause*. This is a region where the total pressure of the magnetosheath balances the magnetic pressure of Earth's magnetic field. The IMF cannot always interact with the terrestrial magnetic field due to the frozen-in condition. However, under certain IMF directions, the magnetic field of the IMF and the terrestrial one will be oppositely directed and may result in a reconnection event. When magnetic reconnection happens, the frozen-in condition breaks down, and the plasma of the solar wind and that of the terrestrial magnetosphere can mix. Such events can lead to auroras seen from the polar region of Earth. Inside the magnetopause is the *magnetosphere*, which is the region where the terrestrial magnetic field dominates. The kinetic pressure of the solar wind results in a compression of the field on the dayside, and a stretching of the magnetosphere on the nightside, called the *magnetotail*.

# Chapter 3

# Spacecraft missions

Before ca. 1960, space could only be studied remotely. As technology has evolved, it has brought space closer to us scientifically. Using spacecraft, we are able to investigate the complex dynamics and processes using in situ measurements.

## 3.1 The Cluster mission

To study the three-dimensional nature of the plasma structures and phenomena existing in the Earth's magnetosphere and space environment, the ESA Cluster mission was launched in 2000 and consisted of four satellites in a (mostly) tetrahedral configuration. Over the years the shape of the tetrahedron and the spacing between the satellites have varied. Cluster has a polar orbit, and during a year, the satellite observes the inner magnetosphere, the polar cusp, the magnetotail, and auroral zones in addition to the solar wind and bow shock. The goal of the mission was to study the small-scale plasma structures occurring in these regions, with the possibility of three-dimentional spatial resolution (Escoubet et al., 2001). The shape of the satellites is approximately cylindrical, with a diameter of 2.9 m and a height of 1.3 m. All four satellites have identical instrumentation to measure various plasma parameters such as the particle distribution of ions and electrons, electric field, and magnetic field (although some instruments have failed during different stages of the mission). The satellites carry 11 instruments, listed in Table 3.1. Figure 3.1 shows a sketch of one of the Cluster satellites. The FGM, CIS, and WHISPER instruments, which are mainly used in this thesis, are marked in green, blue, and purple, respectively, and will be described in more detail below.

### Fluxgate magnetometer (FGM)

The FGM is an instrument used to measure the magnetic field in the space environment (Balogh et al., 1997). It consists of two triaxial fluxgate magnetic

Table 3.1: Summary of the eleven instruments onboard the four Cluster satellites. *Adapted from (Escoubet et al., 2001).*

| Instrument | Subject |
|---|---|
| ASPOC | Spacecraft potential control |
| CIS | Ions |
| DWP | Wave processor |
| EDI | Plasma drift velocity |
| EFW | Electric field and waves |
| FGM | Fluxgate magnetometer |
| PEACE | Electrons |
| RAPID | High energy electrons and ions |
| STAFF | Magnetic and electric fluctuations |
| WBD | Electric field and wave forms |
| WHISPER | Electron density and waves |

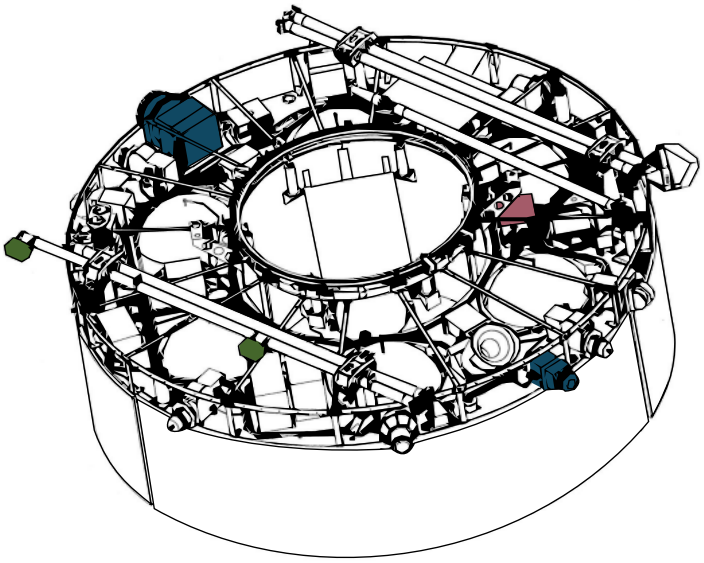

Figure 3.1: Sketch of one of the Cluster satellites with instrumentation. The green marks the FGM instrument, the blue the CIS instrument, and the purple the WHISPER instrument. Adapted from (Ellwood, 1993).

field sensors, where one, the outboard (OB) is located on the end of a 5.2 m long radial boom and the other, the inboard (IB), 1.5 m inboard from the end of the spacecraft. They measure the three components of the field, capturing both the background DC field and the fluctuating field. The OB sensor has mostly been used as the primary sensor. There are six operational ranges of the magnetometer to facilitate good resolution in different magnetic environments, such as the solar wind, with the lowest expected field magnitudes around 3-30 nT, and the magnetosphere, with the highest expected values reaching 1000 nT. The default sampling rate for the primary sensor is 201.75 vectors/second, but this exceeds the telemetry rate allocation. The data is, therefore, convolved to a lower resolution, which is either 22 or 67 Hz.

### Cluster ion spectrometer (CIS)

CIS is an ion composition experiment that measures ion plasma properties such as the full three-dimensional ion distribution (Rème et al., 2001). It consists of two instruments; the Hot Ion Anlyser (HIA) and the ion COmposition and DIstribution Function analyser (CODIF). The instruments have two geometric factors: a high-sensitivity (HS) side for measurements in the magnetosphere with low ion flux levels and a low-sensitivity (LS) side for measurements in the solar wind and magnetosheath with high ion fluxes. CIS-HIA sensors are located on the side of the spinning spacecraft, sampling the ion distribution function in slices with 180 degrees coverage in the polar direction. As the spacecraft rotates, the sensors sample slices of the distribution in different directions to get full coverage. Hence, the resolution of the instrument is one full three-dimensional ion distribution per spin, meaning every 4 seconds. The energy range of CIS-HIA is $\sim$5 eV/e $-$ 32 keV/e. To allow for the detection of the narrow solar wind beam, the LS side is divided into 16 sectors, with 8 around the spin plane with a resolution of 5.625°, and the remaining resolution of 11.25°. The HS is also divided into 16 sectors, but all with a resolution of 11.25° each. CIS-CODIF is a mass-resolving spectrometer with high-sensitivtiy. The resolution is the same as for the HIA instrument. It can resolve the major ion species such as $H^+$, $He^{++}$, $He^+$ and $O^+$. The energy range is between 25 eV/e and 40 keV/e. The angcular resolutions are eight 22.5° sectors for the HS side, while only six sectors (two blind) 22.5° for the LS side. From the distribution functions, the moments are calculated (see Section 2.3); these include density, bulk velocity vector, pressure tensor, and two-component temperature (parallel and perpendicular).

### WHISPER

The WHISPER (Waves of HIgh frequency Sounder for Probing of Electron density by Relaxation) instrument is used for studying the electric field spectra (Décréau et al., 1997). The electric field spectra range in frequency from 2 to 80 kHz with

a resolution of 2.2 s. From the field spectra, the electron density can be deduced from the characteristics of natural occuring waves.

# Chapter 4

# Spacecraft data analysis methods

Several methods have been developed to study the properties of the plasma using single and multiple spacecraft measurements. In this chapter, the methods used in this thesis are presented.

## 4.1 Rankine-Hugoniot conditions

Let us go back to the MHD plasma consideration presented in Chapter 2. The bow shock is the transition where the solar wind is shocked and decelerated from supersonic to subsonic velocities. As a result of the MHD conservation laws, there are jump conditions that relate the plasma parameters on each side of the shock. These jump conditions are also called the Rankine-Hugoniot relations (e.g., Baumjohann and Treumann 2012; Priest 2012).

Assuming a one-dimensional, time stationary shock and a plasma that is described with ideal MHD equations and an isotropic pressure tensor, the jump conditions are:

$$\mathbf{n} \cdot [\rho \mathbf{v}] = 0 \tag{4.1}$$

$$\mathbf{n} \cdot [\rho m \mathbf{v}\mathbf{v}] + \mathbf{n} \left[ p + \frac{B^2}{2\mu_0} \right] - \frac{1}{\mu_0} \mathbf{n} \cdot [\mathbf{B}\mathbf{B}] = 0 \tag{4.2}$$

$$\mathbf{n} \times [\mathbf{v} \times \mathbf{B}] = 0 \tag{4.3}$$

$$\mathbf{n} \cdot [\mathbf{B}] = 0 \tag{4.4}$$

where the brackets, [], denote the difference between upstream (solar wind) and downstream (magnetosheath) values. Here $\mathbf{n}$ is the shock normal direction, $\rho$ is the density, $\mathbf{v}$ the plasma flow velocity, $p$ the pressure and $\mathbf{B}$ is the magnetic field. These relations can be used to predict the downstream values from the upstream ones (or vice versa). These conditions can be simplified by using a reference frame moving with the shock in the shock tangential direction so that

the upstream magnetic field is parallel to the upstream plasma flow velocity. This is known as the de Hoffman-Teller (dHT) frame. In the dHT frame, if the upstream conditions are known, the downstream parameters can be solved:

$$\frac{\rho_d}{\rho_u} = X \tag{4.5}$$

$$\frac{v_{dn}}{v_{un}} = \frac{1}{X} \tag{4.6}$$

$$\frac{v_{dt}}{v_{ut}} = \frac{v_u^2 - v_{Au}^2}{v_u^2 - X v_{Au}^2} \tag{4.7}$$

$$\frac{B_{dn}}{B_{ut}} = \frac{X(v_u^2 - u_{Au}^2)}{v_u^2 - X u_{Au}^2} \tag{4.8}$$

$$\frac{p_d}{p_u} = X + \frac{1}{2}(\gamma - 1) X M_{su}^2 v_u^2 (1 - \frac{v_d^2}{v_u^2}) \tag{4.9}$$

and the problem is reduced to a two-dimensional problem, where $u$ and $d$ refer to upstream and downstream values, and $n$ and $t$ are normal and tangential components. $v_A$ is the Alfvén velocity, $M_s$ the sonic Mach number. $X$ denotes the shock compression ratio.

This was applied when comparing the observations of the same MH observed in the magnetosheath and in the solar wind in Paper I.

## 4.2 Minimum variance analysis

Minimum variance analysis (MVA) is a useful method for studying magnetic field discontinuities and identifying the direction that is approximately normal to the surface. The method can be used for events that can be approximated as a one-dimensional problem, where the gradient is zero in all except one direction, and time stationarity is assumed. With these assumptions, the problem can be expressed as finding the coordinate system where

$$\nabla \cdot \mathbf{B} = \frac{\partial B_z}{\partial z} = 0 \tag{4.10}$$

Here ($x$, $y$, and $z$) are local cartesian coordinates, where the $z$ direction is the $\hat{\mathbf{n}}$ normal direction. From this, $\hat{\mathbf{n}}$ is found by minimizing the variance

$$\sigma^2 = \frac{1}{M} \sum_{m=1}^{M} |(\mathbf{B}^{(m)} - \langle \mathbf{B} \rangle) \cdot \hat{\mathbf{n}}|^2 \tag{4.11}$$

with the constraint that $|\hat{\mathbf{n}}|^2 = 1$ to find the minimum, intermediate, and maximum direction. $M$ is the number of data points in the time series, and $\langle \mathbf{B} \rangle$ is the average magnetic field over the time series. This problem reduces to an eigenvalue problem which in matrix form is given as

$$\sum_{\nu=1}^{3} M^B_{\mu\nu} n_\nu = \lambda n_\mu \tag{4.12}$$

$$M^B_{\mu\nu} = \langle B_\mu B_\nu \rangle - \langle B_\mu \rangle \langle B_\nu \rangle \tag{4.13}$$

where $\mu, \nu = 1, 2, 3$ denote the cartesian components along in the Geocentric Solar Ecliptic (GSE) system, and $M^B_{\mu\nu}$ is the magnetic variance matrix. $\lambda$ are the three eigenvalues, $\lambda_1, \lambda_2, \lambda_3$, for the maximum, intermediate, and minimum variance. These values represent the variance in the magnetic field and are used as a measure of how well the vectors are determined. If all the eigenvalues are of decreasing values, the system is said to be non-degenerate and all three vectors are well determined. If two or more of the eigenvalues are similar, then the exact direction of the corresponding vector is not well defined. More details on this method can be found in (Paschmann and Daly, 1998).

Figure 4.1 shows an example where the MVA method has been applied to a linear MH in the solar wind measured by one of the Cluster spacecraft. The top panel shows the components of the magnetic field in GSE coordinates. The second panel shows the magnetic field in the MVA coordinate system. The two bottom panels show hodograms of the three components, which is a way to visualize the results and identify the polarization of the analyzed structure. The eigenvalues ($\lambda$), eigenvalue ratios and eigenvectors ($\mathbf{x}$) are printed in the right corner.

## 4.3 Timing analysis

When four spacecraft measurements are available, the different observations of the same structure can be used to derive information about the velocity of a structure, in our case a magnetic hole. There are certain assumptions underlying this. One is that the structure can be approximated as a locally planar discontinuity. For mirror mode waves this was described in (Horbury et al., 2004), and applied to magnetic holes in Paper II of this thesis. Knowing the times $t_i$ and positions $r_i$ of the MH in all four spacecraft $i$, the velocity of the MH can be determined. The position and velocity are related as

$$v_t(t_j - t_i) = (\mathbf{r_j} - \mathbf{r_i}) \cdot \mathbf{\hat{n}_t} \tag{4.14}$$

where $i$ and $j$ refer to different spacecraft, and t refers to this being the timing-derived velocity and normal vector. This equation states that the velocity is given by the difference in position along the timing normal, and this method can, therefore, only measure the speed of the structure along the timing normal. The motion perpendicular to it is unknown. Assuming MH are tube like, as described for mirror mode structures in (Horbury et al., 2004), the timing normal will be directed as illustrated in Figure 4.2. Both the velocity and the timing

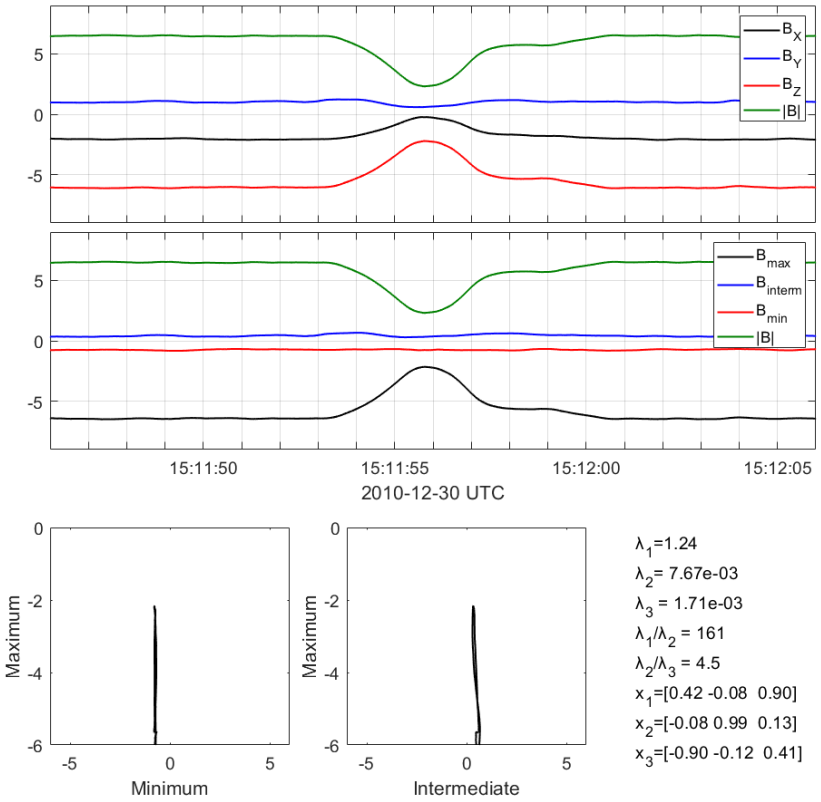


Figure 4.1: Example of MVA applied to a linear MH. Here min, interm and max are the minimum, intermediate and maximum components. All axes (except the time) is in units of nT.

normal are unknown, and the system is simplified by introducing the slowness vector $\mathbf{m}$ given as

$$\mathbf{m} = \frac{\hat{\mathbf{n}}_\mathbf{t}}{v_t} \tag{4.15}$$

Thus, Equation 4.14 reduces to

$$(t_j - t_i) = (\mathbf{r_j} - \mathbf{r_i}) \cdot \mathbf{m} \tag{4.16}$$

Choosing one spacecraft as a reference, $\mathbf{m}$ can easily be estimated. One can also treat Equation 4.16 as an overdetermined system of equations and determine the velocity by minimizing the quadratic error defined as

$$m_l = \frac{1}{2N^2} \left[ \sum_{\alpha=1}^{N} \sum_{\beta=1}^{N} t_{\alpha\beta}(r_{\alpha k} - r_{\beta k}) \right] R_{kl}^{-1} \tag{4.17}$$

$$\mathbf{R_{jk}} = \frac{1}{N} \sum_{\alpha=1}^{N} r_{\alpha j} r_{\alpha k} \tag{4.18}$$

where $N$ is the total number of spacecraft (SC) available, which for Cluster is 4. $\mathbf{R}$ is the volumetric tensor, related to the size and shape of the spacecraft configuration. $t_{\alpha\beta}$ is the time difference between two spacecraft measurements of a structure, often determined using a cross-correlation method. A condition for this method to be used is that the spacecraft formation is not coplanar.

Figure 4.3 shows an example where the timing analysis has been applied to a linear (left side) and rotational (right side) MH. The first panel shows the original times series from the spacecraft. The second panel shows the time-shifted observations. The third panel shows the components of one SC, and the two bottom figures show the SC position together with the magnetic field and the estimated normal vector.

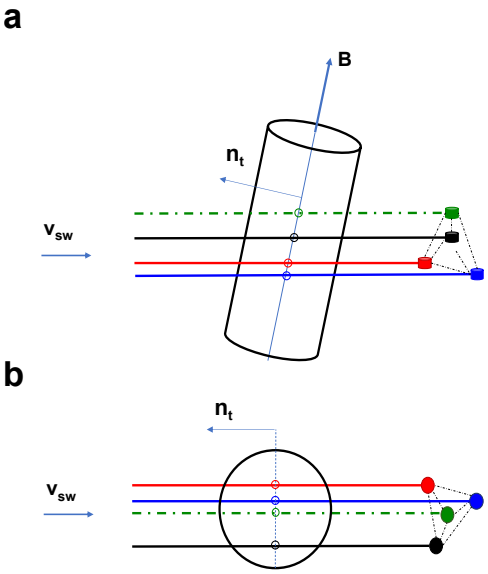


Figure 4.2: Illustration of the geometry and approximation of MH and the timing normal. Reproduced from Paper II and adapted from (Horbury et al., 2004).

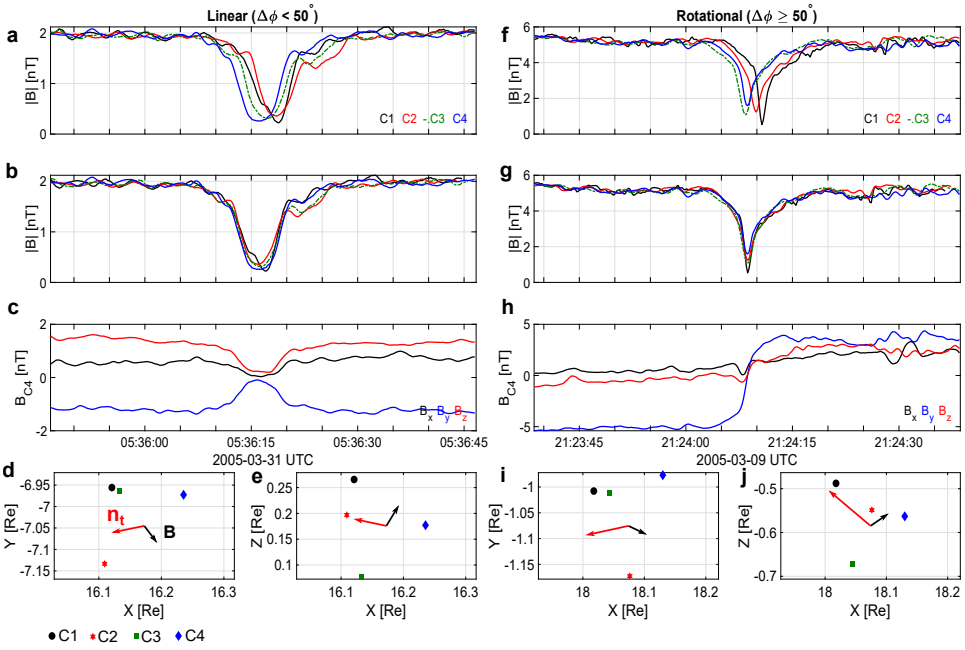


Figure 4.3: Example of the timing analysis applied to a linear MH (left) and a rotational one (right). Reproduced from Paper II.

# Chapter 5

# Magnetic holes

The focus of this thesis work has been magnetic holes. They are localized depletions of the magnetic field magnitude observed in the solar wind and magnetosheath of planets. The term *magnetic hole* was first used by (Turner et al., 1977). Since then, there have been many studies focusing on magnetic holes, and in this chapter, some of that work is summarized.

## 5.1 Definition

Since first reported, magnetic holes (MH) have been defined as localized deep depletions of the magnetic field magnitude. The exact definition has varied, but mostly used is a reduction of more than 50% of the background field. In literature, similar observations of magnetic field decreases have been given different names such as "magnetic depressions", "dropouts", "cavities", "magnetic bubbles" and "isolated mirror modes". In this work, we will use the term "magnetic hole", which, in our understanding, are isolated structures, often observed in connection with mirror mode structures, with time scales of the order of 1-10 s seconds. In addition, we only consider ion-scale magnetic holes that are considerably larger than the ion gyro radius. While sub-ion scale magnetic holes (e.g., Wang et al. 2021a) have also been observed, they are not considered here.

It is common to divide MH into two categories, depending on the rotation of the magnetic field across the hole. Linear MH show little to no rotation; the limit is often set between 10° and 15°. Rotational MH have a larger rotation of the magnetic field, and the limit is often set to above 50°. They have a similar appearance in the magnetic field magnitude, and studies show that the overall characteristics, such as time duration and relative field decrease, are also similar to those of linear MH (Turner et al. 1977, Winterhalter et al. 1994, Karlsson et al. 2021). In the first two papers in this thesis, both linear and rotational MH are considered, while the last two only consider linear MH.

## 5.2 Linear magnetic holes

Table 5.1 summarizes observations of linear MH in the solar wind over the years.

### Location

Linear MH in the solar wind have been observed at a range of heliospheric distance, from as close as 0.17 AU using the Parker Solar Probe (Yu et al., 2021), to the heliosheath using Voyager 1 (Burlaga et al., 2007). Detection in the magnetosheath has been more challenging due to the more turbulent environment, but a few studies have also been focused on observations in planetary magnetosheaths (e.g., Karlsson et al. 2021). MH have also been observed in the coma of a comet (Plaschke et al., 2018).

### Occurence rate

The occurrence rate in the solar wind varies depending on location in the heliosphere, with a possible tendency for a decrease in occurrence rate with increasing heliocentric distances, as can be seen in column three of Table 5.1. At Earth the occurrence rate is reported to be around 1-2 per day (e.g., Turner et al. 1977; Xiao et al. 2014; Volwerk et al. 2021), at Mercury, between 3-4 per day (e.g., Volwerk et al. 2020; Karlsson et al. 2021) and at Mars 5.2 per day (Madanian et al., 2020). However, selection criteria vary between the studies which will affect the occurrence rate.

### Scale sizes

Several studies have looked at the temporal scale size of MH across a range of heliocentric distances. When converting to spatial scales from temporal ones, it has implicitly been assumed that the MH is frozen in to the plasma, having no velocity in the solar wind frame. Hence, the conversion from temporal to spatial scale has been assumed to be straightforward. This is however not obvious, and in some of the suggested formation theories (Section 5.3), they have a non-zero velocity in the solar wind frame. The fourth and fifth columns of Table 5.1 show the temporal scale and the corresponding spatial scale in terms of the local ion gyro radius. The scales vary from a few seconds in the inner heliosphere to several seconds up to hours in the outer heliosphere and heliosheath. Here, it is also important to mention that the identification criteria varies between studies. In newer observations, it is common to use a smoothed average for the magnetic field when identifying MH, often with a window size of 300 s, which also limits the identified scales. The study by (Sperveslage et al., 2000) which used a consistent identification criterion on a dataset spanning a large interval of heliocentric distances, shows a tendency for an increase in the temporal scale of MH for increasing heliospheric distances. The same trend can be seen in the

summary of observations in Table 5.1. However, the scale in terms of ion gyro radius does not show the same trend.

MH are often classified based on their size relative to the ion gyro radius. For scales smaller than $\rho_i$, it is usually referred to as a sub-ion scale MH, or a kinetic scale MH. In this thesis, we only consider larger scale MH considerably larger than the ion gyro radius.

The 3D morphology of ion-scale magnetic holes has not been studied in detail before. With single spacecraft measurements, the 3D morphology can only be studied with strong assumptions related to orientation with respect to known vectors such as the plasma flow velocity and magnetic field. This was done in (Zhang et al., 2008b) and (Xiao et al., 2010) at 0.72 and 1 AU respectively. They found the scale of MH where the solar wind velocity was parallel to the magnetic field to be 2.5 and 1.8 times those where the magnetic field was close to perpendicular. However, this compares the scales of separate MH with each other, and without using multipoint measurements, one cannot know if this holds. In (Fitzenreiter and Burlaga, 1978), the curvature of a MH was studied using simultaneous observations by two spacecraft, with a separation over 30 times the width of the MH. They concluded that the MH observed were separated from the surrounding solar wind by thin current sheets, with little curvature over the scale.

There have been some studies on the 3D morphology of sub-ion scale MH. In (Wang et al., 2020) the morphology is related to the MVA coordinate system. They find that the cross section is circular and suggest that MH are rotational ellipsoids. In (Sundberg et al., 2015) they define a new coordinate system, where one axis is along the magnetic field, and one is along the projection of the velocity in the perpendicular plane. They conclude that the sub-ion MH are aligned along the magnetic field to within a few degrees, with parallel scales $\sim$ 200 km. They also conclude that the MH are circularly symmetric in the plane perpendicular to $\mathbf{B}$.

Table 5.1: Summary of statistical studies and results of linear MH. Based on Table 1 in (Volwerk et al., 2023). The * indicates that the values are estimated from figures in the respective papers.

| Location | Spacecraft | Occ. rate (per day) | Width (s) | Width ($\rho_i$) | Years | References |
|---|---|---|---|---|---|---|
| 0.166-0.82 AU | Parker Solar Probe | 8.7 | 8 (2-28) | | 2018-2019 | (Yu et al., 2021) |
| Mercury 0.4 AU | MESSENGER | 4.4 | 4.6 (2-10) | 29 (17-50) | 2011-2015 | (Karlsson et al., 2021) |
| Mercury - Venus 0-4 - 0.72 AU | MESSENGER | 3.3-1.0 | 7* (4-30) | | 2007-2011 | (Volwerk et al., 2020) |
| Venus 0.72 AU | Venus Express | 4.2 | 5 (across) 13 (along) | 47 (across) 107 (along) | 2006 | (Zhang et al., 2008a) |
| Mercury - Earth 0.3-1 AU | Helios 1 and 2 | 2.2-1.7 | 8 (1-10)* | 37 | 1974-1976 | (Sperveslage et al., 2000) |
| Mercury - Earth | BepiColombo | 3.0 $\pm$ 1.2 | | | 2018-2022 | (Volwerk et al., 2023) |
| Earth L1 | WIND | 0.6 | | (20-1000)* | 1994-2004 | (Stevens and Kasper, 2007) |
| Earth | Imp I/ Explorer 43 | 1.5 | 50 (2-130) | 150 | 1971 | (Turner et al., 1977) |
| Earth | Cluster | 1.8 | 5.5 (across) 10 (along) | | 2001-2009 | (Xiao et al., 2014) |
| Earth | MMS | (2.3) 0.9 | 5-15 | 5-20 | 2017-2019 | (Volwerk et al., 2021) |
| High solar latitude 1-5.4 AU | Ulysses | 5.2 | 22 (5-80) | | 1990-1992 | (Winterhalter et al., 1994) |
| Mars 1.52 AU | MAVEN | 2.1 | 15.5 (1-50)* | (1-100)* | 2016 | (Madanian et al., 2020) |
| 2-17 AU | Voyager 2 | $\sim$ 0.5-0.1 | 32 (20-60)* | 23 (10-30)* | 1978-1985 | (Sperveslage et al., 2000) |
| Heliosheath $\sim$ 94 AU | Voyager 1 | 2-3 | 2.3 hours | 78 (40-117) | 2006 | (Burlaga et al., 2007) |

## 5.3 Formation and origin

As magnetic holes are observed at various distances and environments, exactly where and how they are formed are still open questions. There are a few theories that will be presented below.

### The mirror instability and mirror mode waves

One of the leading theories is that magnetic holes are related to the mirror instability. In observations and simulations, the mirror instability develops as a wave train consisting of peaks and/or dips.

The mirror instability was originally derived from fluid theory and is considered a macroinstability as it affects large plasma volume with slow changes to the macroscopic plasma parameters. However, due to the importance of the single particle motion along and perpendicular to the magnetic field, kinetic methods are needed to describe the instability fully (e.g., Southwood and Kivelson 1993; Kivelson and Southwood 1996). The instability is derived from the kinetic dispersion relation of magnetized plasma waves in the very-low-frequency limit ($\omega << \omega_{gi}$, $k\rho_i << 1$). Here we will not go into more detail on the derivation (for more details see (Treumann and Baumjohann, 1997) Chapter 3.5 and (Baumjohann and Treumann, 2012) 10.6). The resulting dispersion relation is (Equation 3.88 in (Treumann and Baumjohann, 1997)):

$$i\left(\frac{\pi}{2}\right)^{1/2}\frac{\beta_{i,\perp}^2}{\beta_{i,\parallel}}\frac{\omega}{k_\parallel v_{th,i\parallel}} = 1+\sum_s\left(\beta_{s,\perp}-\frac{\beta_{s,\perp}^2}{\beta_{s,\parallel}}\right)+ \\ +\frac{k_{\parallel^2}}{k_\perp^2}\left[1+\frac{1}{2}\sum_s(\beta_{s,\perp}-\beta_{s,\parallel})\right] \tag{5.1}$$

Here, $\beta$ is the plasma beta described Section 2.1, $\omega$ is the angular wave frequency, and $k$ the wave number and $v_{th}$ is the thermal velocity described in Chapter 2. As was done in Chapter 2, $s$ denotes the particle species. The frequency is purely imaginary (no oscillation, only growth/damping) and only depends on the ion component of the plasma. There are two solutions to the dispersion relation. One is for a parallel propagating wave, where the second term in the brackets dominates, and the fire hose instability sets in. The second is for a wave propagating close to perpendicular to the magnetic field, the first term in the brackets dominates and the mirror instability is excited. The instability condition then becomes

$$\sum_s\frac{\beta_{s,\perp}^2}{\beta_{s,\parallel}} > 1+\sum_s\beta_{s,\perp} \tag{5.2}$$

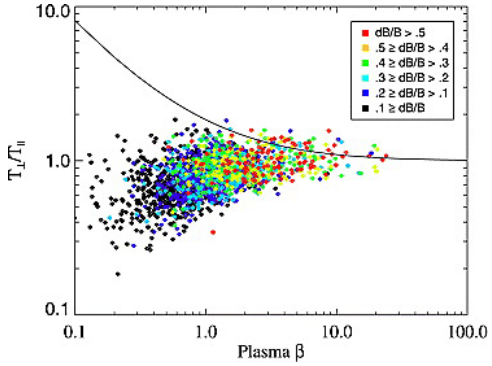


Figure 5.1: Scatterplot of ion anisotropy versus $\beta$ for observations of magnetic holes in the solar wind, where solid line indicates the instability threshold (Stevens and Kasper, 2007).

which, for a single bi-Maxwellian ion species distribution yields an instability threshold, $R_{mm}$ where the instability is exited when

$$R_{mm} = \frac{T_{i,\perp}/T_{i,\parallel}}{1 + 1/\beta_{i,\perp}} > 1 \tag{5.3}$$

The instability threshold is often expressed as the dependence on the temperature ratio over the plasma beta, as seen in Figure 5.1 (Stevens and Kasper, 2007). Here, the instability threshold is given by the solid line, and the MH observations are the colored dots. This study of solar wind MH shows that there is a tendency for deeper MH to be located near the instability threshold, while weaker ones occur in more stable conditions (Stevens and Kasper, 2007).

The physical interpretation of the mirror instability is that due to the increased perpendicular thermal pressure, the magnetic field has a local expansion. This results in the magnetic field having a configuration similar to a magnetic bottle, where particles are trapped in a magnetic mirror configuration, explained in Section 2.2 of Chapter 2. The pressure balance is maintained, and as the magnetic field decreases, due to the expansion, the thermal pressure increases. This is often observed as an anti-correlation of the density or temperature and magnetic field magnitude (e.g., Soucek et al. 2008). The observation of mirror modes is illustrated in Figure 5.2.

### Scale sizes

The wavelength at maximum growth rate gives a theoretical estimate for the scale sizes of mirror mode structures. Following linear theory of the mirror instability (e.g., Hellinger 2007), the wave number for maximum growth rate near the threshold is

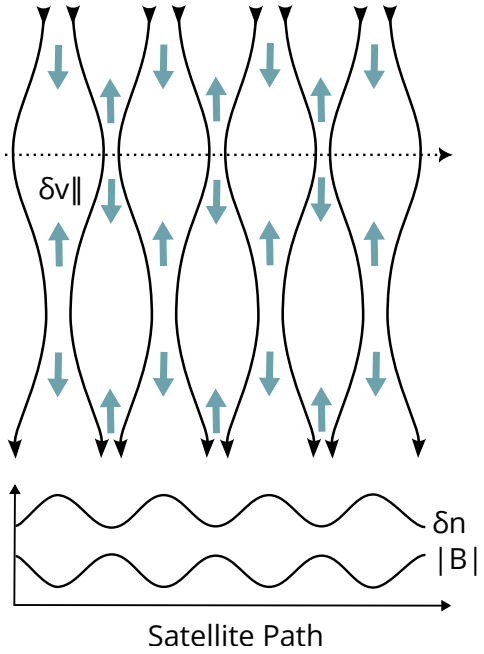


Figure 5.2: Illustration of mirror mode wave train and resulting observation along spacecraft path. Adapted from (Treumann and Baumjohann, 2018).

$$k_{i\perp} = \frac{1}{\rho_{i\perp}}\sqrt{\frac{\Gamma}{6}}, \quad k_{\parallel} = \frac{1}{\rho_{i\perp}}\frac{1}{2\sqrt{6}}\frac{\Gamma}{\sqrt{\Pi}} \tag{5.4}$$

or as expressed in (Horbury and Lucek, 2009) as magnitude

$$|k| = \frac{1}{\rho_{i,\perp}}\sqrt{\frac{\Gamma}{6}\left[1 + \frac{\Gamma}{4\Pi}\right]} \tag{5.5}$$

and the angle between the wave vector and the magnetic field

$$\tan(\theta_{kB}) = 2\sqrt{\frac{\Pi}{\Gamma}} \tag{5.6}$$

where

$$\Gamma = \beta_{i\perp}(\frac{T_{i\perp}}{T_{i,\parallel}} - 1) - 1, \quad \Pi = 1 + \frac{\beta_{i,\perp} - \beta_{i,\parallel}}{2} \tag{5.7}$$

and $\rho_{i,\perp}$ is the proton gyroradius. The predicted wavelength along the magnetic field is estimated to be much larger than that across the field and hence predicts elongated structures approximately oriented along the magnetic field

(Kivelson and Southwood, 1996). If one were to use typical values in the solar wind close to the instability threshold (Figure 6 in (Stevens and Kasper, 2007), $\beta$=4, $T_\perp/T_\parallel = 3.4$), the ratio of parallel and perpendicular wave number is $\sim 12$.

The morphology of mirror mode waves in the magnetosheath was studied in (Horbury and Lucek, 2009). They find that the ratio between the shortest to largest scales of the structures is typically between 2-6, and that the longest direction typically is directed 25° from the maximum variance direction. In addition, the study suggests that the shortest scale is close to parallel to the local magnetopause normal.

### Observations of mirror mode waves and link to MH

There have been several observations of mirror mode waves in the solar wind and planetary magnetosheaths (e.g., Soucek et al. 2008, Simon Wedlund et al. 2022, Dimmock et al. 2022, Génot et al. 2009, Balikhin et al. 2009). They appear as trains of peaks or dips with temporal scales $\sim$ 10 s (Soucek et al., 2008). The presence of peaks or dips is understood to be linked to the degree of instability of the plasma, where peaks are observed in unstable plasmas while dips appear in marginally stable plasmas (Génot et al., 2009).

A dual-spacecraft observation observed the same mirror mode waves in Earth's magnetosheath (Fazakerley and Southwood, 1994). They argue that the transverse plane of the mirror modes is not necessarily of equal length, but more spacecraft are needed to remove ambiguities.

### Simulations of mirror modes link to MH

Simulations of mirror mode waves show that the nonlinear evolution of mirror instability typically leads to peaks, while far away from the instability threshold, the peaks transform to dips and become stable structures (Kuznetsov et al. 2007, Califano et al. 2008, Porazik and Johnson 2013). In (Shoji et al., 2012), two-dimensional low $\beta$ simulations result in dips at the nonlinear stage, while the three-dimensional simulations result in peaks at the same stage. In high $\beta$ simulations, larger and shallower dips were observed, compared to the peaks. The simulations also show that mirror mode waves can evolve and merge into larger structures and change orientation from the initial mirror mode wave train. The process is explained in terms of an attractive force between diamagnetic currents of parallel dips, finally resulting in the merging of the holes and their associated trapped ions. As the coalescence continues, the holes become larger.

### Analytical description of mirror mode waves

A simple way to visualize how the magnetic field lines associated with mirror mode structures look like, is to use the model described by Constantinescu (2002). They show an analytical solution to the magnetic field perturbation caused by a mirror mode. For the first-order components, the expression yields

$$\delta B_r(r,z) = \frac{2\pi}{\alpha} J_1\left(\frac{\alpha r}{L}\right)\left[a_n \sin\left(\frac{\pi z}{L}\right) - b_n \cos\left(\frac{\pi z}{L}\right)\right] \tag{5.8}$$

$$\delta B_z(r,z) = 2J_0\left(\frac{\alpha r}{L}\right)\left[a_1 \sin\left(\frac{\pi z}{L}\right) - b_1 \cos\left(\frac{\pi z}{L}\right)\right] \tag{5.9}$$

here $J$ is the Bessel function, $L$ is the length of the structure. $\alpha$, $a_n$ and $b_n$ are constants. The first is the adimensional quantity (related to the anisotropy), and the remaining are the real and imaginary parts of the Fourier coefficient. This model has been tested and compared to Cluster observations of mirror modes in the terrestrial magnetosheath (Constantinescu et al., 2003).

### Solar wind turbulence

A recent study using hybrid simulations of solar wind turbulence shows that MH-like structures can develop self-consistently from the initial magnetic field perturbations associated with solar wind turbulence (Arrò et al., 2024). The simulations also revealed isolated regions with enhanced temperature anisotropy and the plasma being mirror unstable inside the MH, making the MH stable for longer periods despite the surrounding turbulence. These MH also show trapped particles consistent with magnetic mirror structures.

### Soliton approach to MH

A theory to explain the stability of MH was first formulated by (Burlaga and Lemaire, 1978). They assume that MH are self-consistent flow features that can exist in plasmas even in the absence of instability. Using one-dimensional Vlasov and Maxwell equations, self-consistent solutions were found (with varying magnetic field rotation), that explained MH as non-propagating, sheet-like, pressure-balanced structures. They explain the observed depression of the magnetic field as a consequence of localized pressure enhancement driving a diamagnetic current. However, the theory does not describe the origin of these pressure enhancements or the stability. Later, this model was expanded (to account for stability) to include one-dimensional wave packets propagating quasi-parallel to the magnetic field in a compressible plasma (Baumgärtel, 1999). This model only applies to strictly linear MH, where the background field is the same on both sides of the MH. The solutions are MHD solutions, which are approximately pressure-balanced and propagate quasi-perpendicular to the magnetic field with velocities small compared to the Alfvén velocity. In regards to size, this soliton model predicts a range of sizes (8-60 $\rho_i$), amplitude, and MVA directions. They mentioned that the solition model does not exclude the mirror instability theory, as they could be combined. It should also be mentioned that both these models are one-dimensional and approximate the MH as sheet like. Later, (Avinash and Zank, 2007) described solitons with a fully nonlinear theory, which was compared

to Voyager 1 observations in the heliosheath. They found that the structures were in approximate pressure balance, moved with a velocity tangential to the magnetic field and a fraction of the Alfvén speed, consistent with observations.

### Other Alfvén mechanisms

In addition to the soliton model of MH, there are also other theories applying Alfvén waves physics.

The existence of large-amplitude right-hand polarized Alfvén waves propagating at large angles to the ambient magnetic field has been tied to the formation of MH (Buti et al., 2001). Using one-dimensional hybrid code to study the nonlinear evolution of Alfvén wave packets, they show how the localized inhomogeneities caused by the Alfvén wave evolve to a magnetic dip. They found that perpendicular propagation is essential to the formation of the MH, while temperature anisotropy was less so. The shape of the resulting magnetic holes are described as "V" or "W" shape, different from the more Gaussian/"U" shape predicted by the mirror instability and soliton approach. The "V" shape more resembles a rotational MH, however it is unclear whether this applies to both linear and rotational MH.

Another suggestion is that phase-steepened nonlinear Alfvén waves and the associated pondermotive force lead to local heating, which in turn results in a magnetic depression from diamagnetic effects (Tsurutani et al., 2002). This model includes both linear and rotational MH. This is based on observations by the Ulysses spacecraft, where they argue that the MH could absorb the wave energy and become convected with the solar wind. Another possible evolution suggested is that they interact with other wave packets causing proton energization and evolution.

### Summary of formation mechanisms

Above, several suggested formation mechanisms of MH were presented. None of these are perfect, and none of the mechanisms provide a full explanation as to how MH are formed. The mirror mode threshold has been estimated in relation to observations of MH in the solar wind (e.g., Winterhalter et al. 1994, Stevens and Kasper 2007, Volwerk et al. 2021). All found that the MH mainly occurred in stable regions ($R_{mm} < 1$). It was early suggested that MH are remnants of mirror mode structures created somewhere upstream of the structure where the remaining wave train has decayed away (Winterhalter et al., 1994). A Bohm-like diffusion has been suggested to explain the evolution from wave trains to isolated structures (Hasegawa and Tsurutani, 2011). However, this would also result in weaker depressions, and MH shows a strong depression of the field.

Simulation shows how the initial mirror mode wave train evolves into larger depressions in the nonlinear stage (Shoji et al., 2012). MH are likely the result of nonlinear processes, supporting why they are often seen in mirror-stable or

marginally stable regions. Mirror instability-related formation processes predict zero propagation velocity in the plasma frame, while the Alfvén-related theories predict a non-zero velocity in the plasma frame.

More recent turbulence simulations show how MH-like structures form due to the turbulent plasma processes, independent of the instability condition (Arrò et al., 2024).

## 5.4 Plasma properties of linear MH

Several studies have investigated the plasma properties of magnetic holes.

### Pressure balance

Studies show that the linear MH are often observed to be in pressure balance (e.g., Winterhalter et al. 1994; Stevens and Kasper 2007; Volwerk et al. 2021). This means that when the magnetic pressure decreases as a result of a weaker field, the thermal pressure increases. This can be associated with either an increase in density or temperature, or a combination of the two. A study using the Magnetospheric Multiscale (MMS) mission classified MH as hot when the temperature increased and cold when the density increased (Volwerk et al., 2021). They also found that independent of category, all observed MH were in pressure balance with surroundings. This was also found for hot MH in the exosphere of Mars (Madanian et al., 2020).

### Velocity

When converting from temporal to spatial scales, it has been assumed that MH are convected with the solar wind. However, if the formation mechanism is related to Alfvén waves rather than mirror modes (Tsurutani et al., 2002), theory predicts a non-zero velocity in the solar wind frame. With multipoint measurements, as shown in Chapter 4, one can derive the velocity of structures in the normal direction. This method was applied to mirror modes waves in the magnetosheath in (Horbury et al., 2004), where they concluded that the observed mirror modes were stationary in the plasma frame, slower than the local wave speeds.

### Currents and pitch angle

Currents are essential in the formation and stability of MH. There have been some investigations into how the currents are carried. In (Haynes et al., 2015) the properties and formations of sub-ion scale magnetic holes are investigated using particle-in-cell simulations. It shows a clear electron vortex inside the sub-ion MH, consistent with an azimuthal current. They also conduct a test-particle experiment to see how the electrons move inside the MH, which clearly shows electrons being trapped and following petal-shaped orbits.

Observations of the velocity distribution of MH in the solar wind close to Earth shows an ion vortex, consistent with a ring-like current consistent with the expected current from mirror mode theory and the stability of the MH (Wang et al., 2021b). In (Yao et al., 2023), an ion vortex was identified inside a MH in the magnetosheath associated with a ring-shaped diamagnetic current.

Simulations of mirror modes have shown how trapped resonant particles with small parallel velocities are significantly cooled, reducing the growth rate at the early stages of the nonlinear development of the instability. At the same time, the non-resonant particles with intermediate pitch angles heat as the instability develops (e.g., Kivelson and Southwood 1996; Califano et al. 2008). In (Soucek and Escoubet, 2011), the ion velocity distribution is studied using observations of mirror modes in the magnetosheath. They find that inside the dips there is an increased particle spectral density for ions with pitch angles between 40°-70° and symmetrically at $110° - 150°$, while the population with pitch angles close to 90° is depleted. Between the dips, regions with increased field strength, there is a weak enhancement of ions with pitch angles close to 90° and depletion at intermediate pitch angles. The results show that enhancements in the ion populations correlated with the dips and are slightly more perpendicular to the critical pitch angle, which is predicted by mirror mode theory. It also shows cooling of trapped particles for small parallel velocities.

In (Wang et al., 2024) two observations of MH in the magnetosheath of Jupiter are presented. In the first event they present, they show that electrons have pitch angles close to parallel or antiparallel of the magnetic field. The second event shows a weak depression, where electrons have pitch angles closer to 90°, suggesting that particles are reflected. They explain the different pitch angle distributions with the first event being a crossing of a MH close to the center, while the second event being a crossing close to the mirror point.

### Electric field

Currents and particle motion can be connected to the presence of electric fields. In the model work by (Burlaga and Lemaire, 1978), electric fields are induced perpendicular to the sheet normal and $\mathbf{B}$ to maintain the quasi neutrality. In (Goodrich et al., 2021), they try to recreate a sub-ion scale MH in the magnetosheath of Venus using observations from the Parker Solar Probe in combination with an electron current vortex model. The induced electric field is derived from the Lorentz equation (Equation 2.5), and when the model is compared to the observation, the depression is very similar, but the electric field orientation does not match. The observed electric field is almost perpendicular to that estimated by the model, which is found for all events considered. In Wang et al. (2022) they use observations from the MMS mission of linear MH and find that there is a strong electron flow accompanied by an enhancement of the electric field in the outermost part of the MH.

### Wave activity

Observations show that MH are often associated with wave activity and can act as generators of whistler waves (Svenningsson et al. 2024, Yao et al. 2023). Using Solar Orbiter, it has also been found that an increase in occurrences of Langmuir waves is associated with MH, both rotational and linear ones (Boldú et al., 2023).

## 5.5 Rotational magnetic holes

Rotational magnetic holes have similarities with linear magnetic holes in appearance, but the difference is that there is a large rotation of the magnetic field across it. Rotational magnetic holes have not been studied as much as linear MH. The rotation of the magnetic field components suggests that they are associated with current sheets. The formation mechanism of rotational magnetic holes is not agreed upon. A suggested mechanism is flux annihilation due to (slow) reconnection at the current sheet associated with the magnetic field rotation (Turner et al. 1977, Zhang et al. 2008b). (Burlaga, 1969) show examples of what they call directional discontinuities and argue that they do not necessarily originate from the sun, but can be created locally in the solar wind. This was supported in a study of larger-scale rotational MH (on the order of minutes to hours) (Zurbuchen et al., 2001). They found that they are likely formed in the heliosphere and not due to flux rope reconnection close to the sun, as the composition signature was not the same as one would expect from solar origin. They also argue that the formation process is likely different for these larger MH compared to the MH on the order of seconds we refer to in our work. The initial description of MH as solitons in (Burlaga and Lemaire, 1978) included both linear and rotational MH, but as mentioned in the previous section, fails to explain the stability of these structures. The later soliton models have been developed strictly for linear MH. The connection to phase-steepened Alfvén waves applies to both linear and rotational MH (Tsurutani et al., 2002).

# Chapter 6

# Summary of the included papers

This chapter contains a summary of the papers included in this thesis.

## 6.1 Paper I - Solar wind magnetic holes can cross the bow shock and enter the magnetosheath

In Paper I we investigate the origin of magnetosheath MH. The bow shock results in downstream temperature anisotropies that can trigger mirror instability, which in turn can result in mirror mode waves that are frequently observed in the planetary magnetosheath. MH have also been observed in the magnetosheath. However it is unclear whether they are the result of local mirror mode excitations or if they are solar wind magnetic holes which can cross the bow shock and enter the magnetosheath. Using the Cluster mission, 26 events were identified where the same MH is observed upstream of the bow shock, and a short time later downstream. We show examples where the upstream and downstream conditions are well described by MHD Rankine-Hugoniot jump conditions. Based on the identified 26 events, we show that both the temporal scale size and magnetic hole rotations are similar upstream and downstream, while the depth varies more. We conclude that the observations are consistent with magnetic holes in the magnetosheath having solar wind origin.

Figure 6.1 shows one of the events from the analysis. The left column shows the spacecraft data where panel (c) shows the MH in the solar wind (observed by Cluster 2) and panels (d) and (e) show the same MH in the magnetosheath (observed by Cluster 3 and 4). In panels (g) to (j) the position of the spacecraft in GSE coordinates are plotted, with a model bow shock indicated. The final panels show the components of the magnetic field from spacecraft 2 and 4 (k) and (i) and the Rankine-Hugoniot predictions in panels (m) and (n). There is also a clear substructure in the MH observed by both spacecraft, supporting that this is the same MH. Here we also see that there is a good agreement between the observed downstream values and the predicted values from the jump conditions.

h

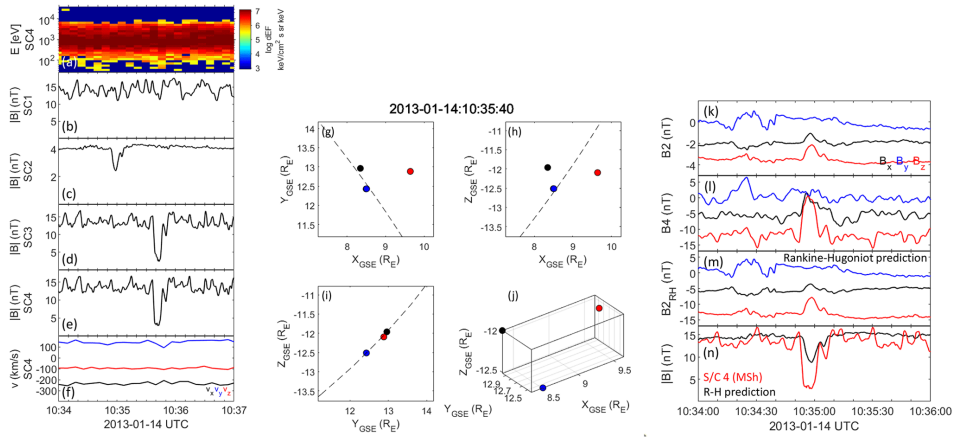


Figure 6.1: Example event used in the study. (a–f) Zoomed-in interval of the same event as Fig. 1. (g–j) Spacecraft position in the same format as Fig. 1. (k–l) Magnetic field components for spacecraft 2 and 4 in the GSE coordinate system, panel (m): RH (Rankine–Hugoniot) prediction for spacecraft 2. (n) RH prediction of magnetic field strength (black) compared with magnetic field strength measured by spacecraft 4. The data for spacecraft 2 have been time-shifted for easier comparison. Reproduced from Figure 2 in Paper I.

**Contribution:** I took part in the analysis of the results, discussions, and editing of the paper.

## 6.2 Paper II - Velocity of magnetic holes in the solar wind from Cluster multipoint measurements

In Paper II, we investigated the velocity of magnetic holes, both linear and rotational, using a timing analysis. The various formation theories predict different propagating velocities, while in most of the literature, MH are assumed to be convected with the solar wind. Using observations from the Cluster mission from 2005, we first identified times when the spacecraft was in the solar wind. The satellite separations were between 600 and 2600 during the first quarter of 2005, providing good conditions for observations of simultaneous passage of the MH over all four SC. Isolated MH were identified by finding times when the relative deviation of the magnetic field was more than 50% of the background. To remove turbulent regions such as the foreshock, the normalized standard deviation over a 30 s moving average was set to be less than 0.15 nT. Then, the identified events were manually inspected to verify that the MH was seen in all four spacecraft. A timing analysis was applied to all events, where the time shift between spacecraft was determined using a cross-correlation technique. From this we found the velocity of the MH along the identified timing normal. To compare this to the plasma velocity we took the projection of the solar wind velocity along the timing normal. The statistical results are shown in Figure 6.2. From our analysis, we conclude that both rotational and linear MH are convected with the solar wind, which for rotational MH is consistent with a magnetic reconnection event and for linear MH, is consistent with the connection to mirror mode waves.

**Contributions:** I organized the study, performed the analysis, and wrote the article with the help of comments from, and discussion with the co-authors.

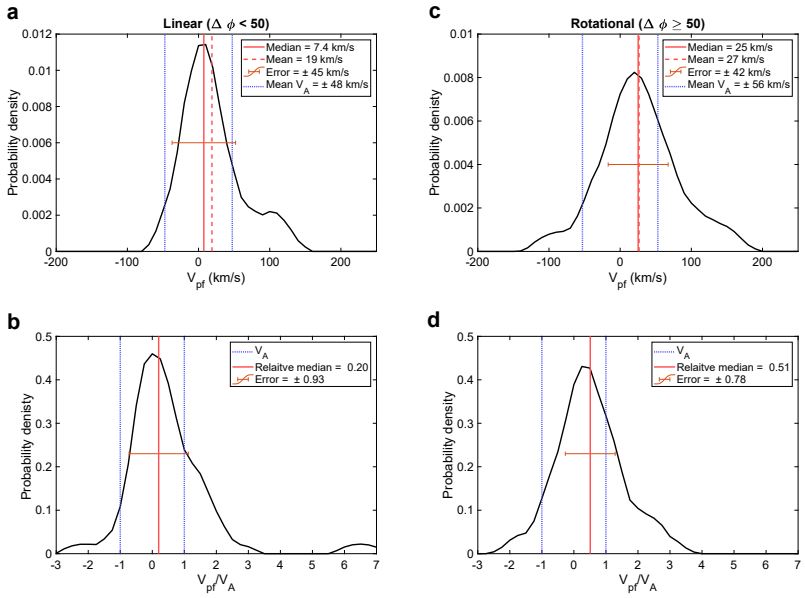


Figure 6.2: Panels (a) and (c) show the probability density of the MH velocity in the plasma frame. Panels (b) and (d) show the results for the MH velocity relative to the local Alfvén velocity. Reproduced from Figure 5 in Paper II.

## 6.3 Paper III - Morphology of magnetic holes: Methodology and case studies

In Paper III, we present a new method of studying the 3D morphology of magnetic holes with four case studies. There have been several studies reporting on the temporal scales using single spacecraft measurement, but there is a lack of studies on the 3D morphology using multispacecraft measurement. The same method as in Paper II has been used to identify the solar wind intervals and MH candidates. The first step in the analysis is to transform into a coordinate system, which is shifted to be in the plasma frame and centered at the deepest observation of the MH. The new coordinate system is defined with one axis initially being along, the maximum variance direction, one perpendicular to the direction of motion, and the final one completing the right-hand system. This coordinate system is then rotated 90° in all directions to identify the coordinate system in which the minima of the four crossings of the magnetic hole align along one direction. The alignment is found if the MH is a regular structure. Several events where the alignment is very good are found, suggesting that the observed MH is regular, and that it is the same MH observed by all four SC. The MH scale sizes along the new axes are determined by fitting a Gaussian to the observations. Figure 6.3 shows one of the events from the analysis in the new coordinate system. The stippled lines are the spacecraft observations and the solid lines are the Gaussian fit. We have also reconstructed the MH by interpolating between the spacecraft observing the MH in the $X - Y$ plane, which is seen in panels (f) and (g). For this event, it is clear that the estimated morphology is a structure that is much longer along the $Z$ axis than in the $X - Y$ plane, which is consistent with mirror mode theory.

**Contributions:** I organized the study, performed the analysis, and wrote the article with the help of comments from, and discussion with the other co-authors.

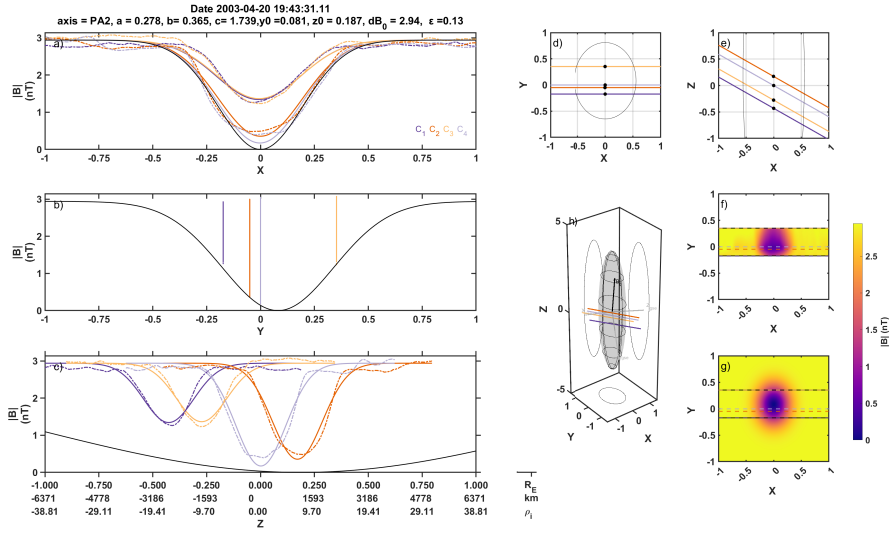


Figure 6.3: Example of the observed MH in the new coordinate system. The stippled lines are the observations and the solid lines are the Gaussian model fit. Reprinted from Figure 10 in Paper III.

## 6.4 Paper IV - Statistical analysis of the morphology of magnetic holes in the solar wind close to 1 AU

In Paper IV we use the same methodology presented in Paper III to make a statistical analysis. Years 2001-2018 of the database of Cluster were searched, and after identifying the most suitable candidates, 442 events were used in the final analysis. The coordinate transformation and alignment were done individually for each event, and a Gaussian model was fitted to the MH using a least-squares method to estimate the scales. The scales are also presented in terms of the separation of the spacecraft along the new axes. With this statistical approach we discovered that the axis in which the observations align is also, in most of the events, the shortest axis. The other two dimensions are harder to determine, as we only have four spacecraft paths. However, our study suggests that these two dimensions are both associated with scales considerably larger than the shortest scale, consistent with a pancake or knife-blade like morphology. This deviates significantly from linear mirror mode theory and indicates that MH are the result of non-linear processes.

The morphology has been estimated by introducing the elongation and planarity factors, which compare the semi-major, intermediate, and semi-minor axis of the MH. Figure 6.4a) illustrates how the elongation and planarity parameters connect to shape, while Figure 6.4b) shows the resulting elongation and planarity for the MH included in the study for a coordinate system where $x$ is in the identified alignment direction and $z$ is along the projection of $\mathbf{B}$ in the $y$-$z$ plane. The colors indicate the ordering from smallest to largest scale, $a$ being along $x$, $b$ being along $y$ and $c$ being along $z$. The colors represent the different ordering from smallest to largest value, i.e $abc$ means that $a$ is the smallest scale and $c$ the largest scale of the MH. The numbers in each square indicate the number of events in each square and the percentage. Over 50% of the events lie in the top part of the planarity, i.e., one direction being smaller than the other two, consistent with pancake or knife-blade like morphology.

**Contributions:** I organized the study, performed the analysis, and wrote the article with the help of comments from, and discussion with the co-authors.

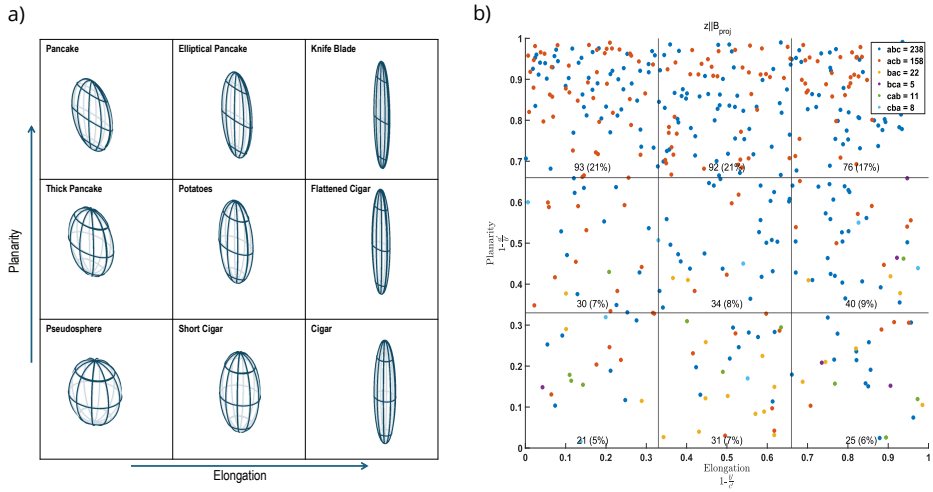


Figure 6.4: a) illustrations of elongation and planarity parameters and estimated shape. b) Result of shape from model fit of all observations. These results are for when one direction is aligned along the projection of **B**. Colors indicate the ordering from smallest to largest scales. Reproduced from Figures 12 and 14ii in Paper IV.

# Chapter 7

# Discussion and outlook

The main aim of this thesis work has been to understand the phenomenon of magnetic holes better. Though there have been many studies of magnetic holes over the decades, there is still no consensus on how and where they are formed. The leading theory is that they are somehow related to mirror mode waves and that they are generated or maintained due to the mirror instability. The observation of MH in a range of heliospheric distances means they are either created locally, or they could be generated close to the sun and convected outwards with the solar wind. In this chapter we will discuss the three objectives stated in the introduction and see how they relate to previous studies and work.

In Chapter 5 different formation mechanisms were introduced. The solar wind is sometimes mirror mode unstable, such as in connection with coronal mass ejections. However, statistically, this is not very common, and observations of MH are often observed below or close to the instability threshold. Possible scenarios of where and how they are generated are thus: (1) Formed close to the sun's photosphere and convected outwards. (2) created when the solar wind is marginally stable, and only one dip formed, rather than a train of dips. This could happen in the presence of turbulence, where small regions of the solar wind plasma could be pushed over the instability boundary into the unstable state. (3) A mirror mode wave train merging together to larger isolated structures. Scenario (1) is not mutually exclusive with (2) and (3).

## 7.1 Origin of magnetosheath MH

MH are also observed in planetary magnetosheath. As mentioned in the Chapter 2, the magnetosheath is a region with high temperature anisotropy and favorable conditions for mirror mode waves, which are often observed (e.g., Horbury et al. 2004; Génot et al. 2009). Hence, it is not unlikely that MH are also created in the magnetosheath and become isolated structures due to similar mechanisms as solar wind MH, i.e mechanisms (2) and (3).

In Paper I, we show that some magnetosheath MH have solar wind origin. However, it is still an open question whether all magnetosheath MH were created in the solar wind. A way to investigate this would be to see if the pressure balance in the upstream observations of the MH is disturbed by the bow shock crossing. If the pressure balance is maintained, these magnetic holes could survive and further interact with the magnetopause.

## 7.2 Velocity of solar wind magnetic holes

Of the different formation mechanisms, some predict MH being frozen-in and convected with the solar wind (mirror mode instability, turbulence). Others predict varying degrees of propagation parallel to the magnetic field (solution, Alfvén waves). Objective 2 is addressed in Paper II, where we used simultaneous observations of the same MH from all four Cluster satellites. The events studied were from the first quarter of 2005, when the Cluster satellites had an apogee in the solar wind and a separation suitable for this study. The events were carefully chosen to ensure that the database contained only isolated MH, and no foreshock structures. We included both rotational and linear MH, setting the boundary for linear and rotational at 50°, based on the distribution. In the paper, we show that the propagation in the solar wind frame is much slower than the Alfvén velocity and actually consistent with zero. This method can, on the other hand, only derive information on the velocity along the timing normal. How the MH moves in the perpendicular plane is not known.

## 7.3 Morphology of magnetic holes in the solar wind

The shape and 3D size of magnetic holes is not well known. As mentioned in Chapter 5, With only one spacecraft the morphology of magnetic holes cannot be established. This is because strong assumptions must be made regarding the alignment with specific vectors, such as the plasma flow velocity and magnetic field. Multipoint measurements allow for investigating this, which has been the focus of Papers III and IV. Confirming that MH are convected with the solar wind in Paper II results in the temporal scales easily being converted to spatial scales.

In Paper III a new method of investigating the morphology is presented. Here we show four MH events with the applied method. We find that the scale along $z$ is more variable than along the other two directions. A Gaussian model is used to estimate the scale, which for these four events works well. In Paper IV this model is expanded and applied to over 400 events. Here, we present the first comprehensive multispacecraft estimate of the morphology of solar wind MH. The statistical result of the model shows that the magnetic field is perpendicular to the shortest scale direction. The connection to the magnetic field clearly indicates a strong relation between the magnetic field and the morphology. This is also

consistent with classic linear mirror mode theory, as linear mirror modes have their longest dimension approximately aligned with the magnetic field. Further, we find that the morphology is typically of high planarity, i.e., pancake/knife-blade shape. This, on the other side, is not consistent with classical linear mirror modes (tube like), which was also found for mirror modes in the magnetosheath (Horbury and Lucek, 2009). This underlines that models and simulations need to account for the full three-dimensional morphology, and not impose symmetrical assumptions.

## 7.4 Outlook

The work presented here is just the beginning of investigating MH with multipoint measurements, and here we will list possible future studies.

The method presented in Paper I could be applied to investigate what happens with a MH in the interaction with the magnetopause. This could also could be compared to ground measurement and investigation of the geomagnetic field. Magnetosheath jets (Plaschke et al., 2018) exhibit scales on the order of 1 $R_E$ and have been demonstrated to influence the magnetosphere. MH have comparable spatial scales, making it plausible that they, too, could impact the near-Earth environment. Future simulation studies could also investigate the magnetopause interaction by comparing the old rotationally symmetric MH model with our suggested morphology. Further, these results could be compared with the observed effects of MH on the magnetopause to see which morphology reproduces the results best.

The work from Paper II could be expanded and applied for the events identified and used in Paper IV, which would provide a larger dataset where the analysis could include the propagation direction. It would also be interesting to apply this method to MH in the magnetosheath as was done or mirror modes in (Horbury et al., 2004).

The method presented in Papers III and IV can also be applied to rotational MH, and other plasma structures such as jets and short large-amplitude magnetic field structures(SLAMS). There is yet to be a statistical study of MH in the terrestrial magnetosheath. It would be interesting to identify MH in the magnetosheath, apply the same analysis, and compare it to solar wind MH. The results from Papers III and IV provide real physical estimates of the scale sizes. This could be combined with future 3D simulations with realisiting solar wind parameters to compare the 3D morphology. This would check out predicted results and possibly be a way to further understand the formation mechanism and origin.

It could be possible to apply machine learning techniques to see if there is any clear distinction in the plasma parameters of linear and rotational MH and investigate if there is any clear boundary between the two classes which again could be tied to the formation.

In this work we have only used the Cluster mission, while it would be interesting to use the MMS mission, with burst data providing very high-resolution data of the ion and electron distribution, to investigate the internal plasma properties of a MH, such as the electric field, current, pitch angles and possibly waves. Using the MMS mission one could also apply the morphology model to sub-ion scale MH, investigating the morphology further.

To have more than four measurement points, the database of events provided from Paper IV could be checked for conjunctions with other satellites near Earth with orbits passing in the solar wind, such as MMS or Themis. Future spacecraft missions, such as the suggested Plasma Observatory, with more than four satellites would improve the estimation of the morphology with the combined high-resolution ion data.

# References


Arrò, G., Califano, F., Pucci, F., Karlsson, T., and Li, H. (2024). Large Scale Linear Magnetic Holes with Magnetic Mirror Properties in Hybrid Simulations of Solar Wind Turbulence. *The Astrophysical Journal Letters*, 970(1):L6. arXiv:2405.18591 [astro-ph].

Avinash, K. and Zank, G. P. (2007). Magnetic structures in the heliosheath. *Geophysical Research Letters*, 34(5):2006GL028582.

Balikhin, M. A., Sagdeev, R. Z., Walker, S. N., Pokhotelov, O. A., Sibeck, D. G., Beloff, N., and Dudnikova, G. (2009). THEMIS observations of mirror structures: Magnetic holes and instability threshold. *Geophysical Research Letters*, 36(3):2008GL036923.

Balogh, A., Dunlop, M., Cowley, S., Southwood, D., Thomlinson, J., Glassmeier, K., Musmann, G., Lühr, H., Buchert, S., Acuna, M., and others (1997). The Cluster magnetic field investigation. *Space Science Reviews*, 79(1):65–91.

Baumgärtel, K. (1999). Soliton approach to magnetic holes. *Journal of Geophysical Research: Space Physics*, 104(A12):28295–28308.

Baumjohann, W. and Treumann, R. A. (2012). *Basic space plasma physics*. World Scientific.

Biermann, L. (1951). Kometenschweife und solare Korpuskularstrahlung. *Zeitschrift für Astrophysik, Vol. 29, p. 274*, 29:274.

Boldú, J. J., Graham, D. B., Morooka, M., André, M., Khotyaintsev, Y. V., Karlsson, T., Souček, J., Píša, D., and Maksimovic, M. (2023). Langmuir waves associated with magnetic holes in the solar wind. *Astronomy & Astrophysics*, 674:A220.

Burgess, D., Lucek, E. A., Scholer, M., Bale, S. D., Balikhin, M. A., Balogh, A., Horbury, T. S., Krasnoselskikh, V. V., Kucharek, H., Lembège, B., Möbius, E., Schwartz, S. J., Thomsen, M. F., and Walker, S. N. (2005). Quasi-parallel Shock Structure and Processes. *Space Science Reviews*, 118(1-4):205–222.

Burlaga, L. and Lemaire, J. (1978). Interplanetary magnetic holes: Theory. *Journal of Geophysical Research: Space Physics*, 83(A11):5157–5160.

Burlaga, L., Ness, N., and Acuna, M. (2007). Linear magnetic holes in a unipolar region of the heliosheath observed by Voyager 1. *Journal of Geophysical Research: Space Physics*, 112(A7).

Burlaga, L. F. (1969). Directional discontinuities in the interplanetary magnetic field. *Solar Physics*, 7(1):54–71.

Buti, B., Tsurutani, B. T., Neugebauer, M., and Goldstein, B. E. (2001). Generation mechanism for magnetic holes in the solar wind. *Geophysical Research Letters*, 28(7):1355–1358.

Califano, F., Hellinger, P., Kuznetsov, E., Passot, T., Sulem, P. L., and Trávníček, P. M. (2008). Nonlinear mirror mode dynamics: Simulations and modeling. *Journal of Geophysical Research: Space Physics*, 113(A8):2007JA012898.

Chen, F. F. and others (1984). *Introduction to plasma physics and controlled fusion*, volume 1. Springer.

Constantinescu, O. (2002). Self-consistent model of mirror structures. *Journal of Atmospheric and Solar-Terrestrial Physics*, 64(5-6):645–649.

Constantinescu, O., Glassmeier, K.-H., Treumann, R., and Fornaçon, K.-H. (2003). Magnetic mirror structures observed by Cluster in the magnetosheath. *Geophysical research letters*, 30(15).

Dimmock, A. P., Yordanova, E., Graham, D. B., Khotyaintsev, Y. V., Blanco-Cano, X., Kajdič, P., Karlsson, T., Fedorov, A., Owen, C. J., Werner, E. A. L. E., and Johlander, A. (2022). Mirror Mode Storms Observed by Solar Orbiter. *Journal of Geophysical Research: Space Physics*, 127(11):e2022JA030754.

Décréau, P. M. E., Fergeau, P., Krannosels'kikh, V., Lévêque, M., Martin, P., Randriamboarison, O., Sené, F. X., Trotignon, J. G., Canu, P., and Mögensen, P. B. (1997). WHISPER, A Resonance Sounder and Wave Analyser: Performances and Perspectives for the Cluster Mission. *Space Science Reviews*, 79(1/2):157–193.

Ellwood, J. (1993). Cluster Experiment Interface Document, Part A. EID A CLEST-RS-0002, issue 2, section 2, page 6, European Space Agency.

Escoubet, C., Fehringer, M., and Goldstein, M. (2001). Introduction the Cluster mission. *Annales Geophysicae*, 19(10/12):1197–1200.

Fazakerley, A. and Southwood, D. (1994). Mirror instability in the magnetosheath. *Advances in Space Research*, 14(7):65–68.

Fitzenreiter, R. J. and Burlaga, L. F. (1978). Structure of current sheets in magnetic holes at 1 AU. *Journal of Geophysical Research: Space Physics*, 83(A12):5579–5585.

Goodrich, K. A., Bonnell, J. W., Curry, S., Livi, R., Whittlesey, P., Mozer, F., Malaspina, D., Halekas, J., McManus, M., Bale, S., Bowen, T., Case, A., Dudok De Wit, T., Goetz, K., Harvey, P., Kasper, J., Larson, D., MacDowall, R., Pulupa, M., and Stevens, M. (2021). Evidence of Subproton-Scale Magnetic Holes in the Venusian Magnetosheath. *Geophysical Research Letters*, 48(5):e2020GL090329.

Génot, V., Budnik, E., Hellinger, P., Passot, T., Belmont, G., Trávníček, P. M., Sulem, P.-L., Lucek, E., and Dandouras, I. (2009). Mirror structures above and below the linear instability threshold: Cluster observations, fluid model and hybrid simulations. *Annales Geophysicae*, 27(2):601–615.

Hasegawa, A. and Tsurutani, B. T. (2011). Mirror Mode Expansion in Planetary Magnetosheaths: Bohm-like Diffusion. *Physical Review Letters*, 107(24):245005.

Haynes, C. T., Burgess, D., Camporeale, E., and Sundberg, T. (2015). Electron vortex magnetic holes: A nonlinear coherent plasma structure. *Physics of Plasmas*, 22(1):012309.

Hellinger, P. (2007). Comment on the linear mirror instability near the threshold. *Physics of plasmas*, 14(8).

Horbury, T. and Lucek, E. (2009). Size, shape, and orientation of magnetosheath mirror mode structures. *Journal of Geophysical Research: Space Physics*, 114(A5).

Horbury, T., Lucek, E., Balogh, A., Dandouras, I., and Reme, H. (2004). Motion and orientation of magnetic field dips and peaks in the terrestrial magnetosheath. *Journal of Geophysical Research: Space Physics*, 109(A9).

Karlsson, T., Heyner, D., Volwerk, M., Morooka, M., Plaschke, F., Goetz, C., and Hadid, L. (2021). Magnetic Holes in the Solar Wind and Magnetosheath Near Mercury. *Journal of geophysical research. Space physics*, 126(5).

Kivelson, M. G. and Russell, C. T., editors (1995). *Introduction to space physics*. Cambridge Univ. Press, Cambridge, 1. publ., transferred to digital print edition.

Kivelson, M. G. and Southwood, D. J. (1996). Mirror instability II: The mechanism of nonlinear saturation. *Journal of Geophysical Research: Space Physics*, 101(A8):17365–17371.

Kuznetsov, E. A., Passot, T., and Sulem, P. L. (2007). Dynamical Model for Nonlinear Mirror Modes near Threshold. *Physical Review Letters*, 98(23):235003.

Madanian, H., Halekas, J. S., Mazelle, C. X., Omidi, N., Espley, J. R., Mitchell, D. L., and McFadden, J. P. (2020). Magnetic Holes Upstream of the Martian Bow Shock: MAVEN Observations. *Journal of geophysical research. Space physics*, 125(1).

Paschmann, G. and Daly, P. W. (1998). Analysis Methods for Multi-Spacecraft Data. *ISSI Scientific Reports Series SR-001, ESA/ISSI*, 1. ADS Bibcode: 1998ISSIR...1.....P.

Plaschke, F., Karlsson, T., Goetz, C., Moestl, C., Richter, I., Volwerk, M., Eriksson, A., Behar, E., and Goldstein, R. (2018). First observations of magnetic holes deep within the coma of a comet. *Astronomy & Astrophysics*, 618:A114.

Porazik, P. and Johnson, J. R. (2013). Gyrokinetic particle simulation of nonlinear evolution of mirror instability. *Journal of Geophysical Research: Space Physics*, 118(11):7211–7218.

Priest, E. R. (2012). *Solar magnetohydrodynamics*, volume 21. Springer Science & Business Media.

Rème, H., Aoustin, C., Bosqued, J., Dandouras, I., Lavraud, B., Sauvaud, J., Barthe, A., Bouyssou, J., Camus, T., Coeur-Joly, O., and others (2001). First multispacecraft ion measurements in and near the Earth's magnetosphere with the identical Cluster ion spectrometry (CIS) experiment. *Annales Geophysicae*, 19(10/12):1303–1354.

Shoji, M., Omura, Y., and Lee, L.-C. (2012). Multidimensional nonlinear mirror-mode structures in the Earth's magnetosheath. *Journal of Geophysical Research: Space Physics*, 117(A8).

Simon Wedlund, C., Volwerk, M., Mazelle, C., Halekas, J., Rojas-Castillo, D., Espley, J., and Möstl, C. (2022). Making Waves: Mirror Mode Structures Around Mars Observed by the MAVEN Spacecraft. *Journal of Geophysical Research: Space Physics*, 127(1):e2021JA029811.

Soucek, J. and Escoubet, C. P. (2011). Cluster observations of trapped ions interacting with magnetosheath mirror modes. *Annales Geophysicae*, 29(6):1049–1060.

Soucek, J., Lucek, E., and Dandouras, I. (2008). Properties of magnetosheath mirror modes observed by Cluster and their response to changes in plasma parameters. *Journal of Geophysical Research: Space Physics*, 113(A4).

Southwood, D. J. and Kivelson, M. G. (1993). Mirror instability: 1. Physical mechanism of linear instability. *Journal of Geophysical Research: Space Physics*, 98(A6):9181–9187.

Sperveslage, K., Neubauer, F. M., Baumgärtel, K., and Ness, N. F. (2000). Magnetic holes in the solar wind between 0.3 AU and 17 AU. *Nonlinear processes in geophysics*, 7(3/4):191–200.

Stevens, M. L. and Kasper, J. C. (2007). A scale-free analysis of magnetic holes at 1 AU. *Journal of Geophysical Research: Space Physics*, 112(A5):2006JA012116.

Sundberg, T., Burgess, D., and Haynes, C. T. (2015). Properties and origin of subproton-scale magnetic holes in the terrestrial plasma sheet. *Journal of Geophysical Research: Space Physics*, 120(4):2600–2615.

Svenningsson, I., Yordanova, E., Khotyaintsev, Y. V., André, M., Cozzani, G., and Steinvall, K. (2024). Whistler Waves in the Quasi-Parallel and Quasi-Perpendicular Magnetosheath. *Journal of Geophysical Research: Space Physics*, 129(6):e2024JA032661.

Treumann, R. A. and Baumjohann, W. (1997). *Advanced space plasma physics*, volume 30. Imperial College Press London.

Treumann, R. A. and Baumjohann, W. (2018). The mirror mode: a "superconducting" space plasma analogue. *Annales Geophysicae*, 36(4):1015–1026.

Tsurutani, B. T., Dasgupta, B., Galvan, C., Neugebauer, M., Lakhina, G. S., Arballo, J. K., Winterhalter, D., Goldstein, B. E., and Buti, B. (2002). Phase-steepened Alfvén waves, proton perpendicular energization and the creation of magnetic holes and magnetic decreases: The ponderomotive force. *Geophysical Research Letters*, 29(24).

Turner, J. M., Burlaga, L. F., Ness, N. F., and Lemaire, J. F. (1977). Magnetic holes in the solar wind. *Journal of Geophysical Research*, 82(13):1921–1924.

Volwerk, M., Goetz, C., Plaschke, F., Karlsson, T., Heyner, D., and Anderson, B. (2020). On the magnetic characteristics of magnetic holes in the solar wind between Mercury and Venus. *Annales Geophysicae*, 38(1):51–60.

Volwerk, M., Karlsson, T., Heyner, D., Goetz, C., Simon Wedlund, C., Plaschke, F., Schmid, D., Fischer, D., Mieth, J., Richter, I., Nakamura, R., Narita, Y., Magnes, W., Auster, U., Matsuoka, A., Baumjohann, W., and Glassmeier, K.-H. (2023). Magnetic holes between Earth and Mercury: BepiColombo cruise phase. *Astronomy & Astrophysics*, 677:A2.

Volwerk, M., Mautner, D., Wedlund, C. S., Goetz, C., Plaschke, F., Karlsson, T., Schmid, D., Rojas-Castillo, D., Roberts, O. W., and Varsani, A. (2021). Statistical study of linear magnetic hole structures near Earth. *Annales Geophysicae*, 39(1):239–253.

Wang, C. Q., Fu, H. S., Cao, J. B., Wang, Z., Fu, W. D., Guo, Z. Z., Lan, H., Sun, T. R., Wei, Y., Ni, B. B., Yao, Z. H., and Zhang, B. Z. (2024). Magnetic Hole and Its Resultant Electron Pitch-Angle Distribution at Jupiter. *Geophysical Research Letters*, 51(20):e2024GL111372.

Wang, G. Q., Volwerk, M., Du, A. M., Xiao, S. D., Wu, M. Y., Chen, Y. Q., and Zhang, T. L. (2021a). Statistical Study of Small-scale Magnetic Holes in the Upstream Regime of the Martian Bow Shock. *The Astrophysical Journal*, 921(2):153.

Wang, G. Q., Volwerk, M., Wu, M. Y., Hao, Y. F., Xiao, S. D., Wang, G., Liu, L. J., Chen, Y. Q., and Zhang, T. L. (2021b). First Observations of an Ion Vortex in a Magnetic Hole in the Solar Wind by MMS. *The Astronomical Journal*, 161(3):110.

Wang, G. Q., Volwerk, M., Xiao, S. D., Wu, M. Y., Chen, Y. Q., and Zhang, T. L. (2022). Electron-Scale Current Sheet as the Boundary of a Linear Magnetic Hole in the Terrestrial Current Sheet Observed by the Magnetospheric Multiscale Mission. *Journal of Geophysical Research: Space Physics*, 127(5):e2021JA029707.

Wang, G. Q., Volwerk, M., Xiao, S. D., Wu, M. Y., Hao, Y. F., Liu, L. J., Wang, G., Chen, Y. Q., and Zhang, T. L. (2020). Three-dimensional Geometry of the Electron-scale Magnetic Hole in the Solar Wind. *The Astrophysical Journal Letters*, 904(1):L11.

Winterhalter, D., Neugebauer, M., Goldstein, B. E., Smith, E. J., Bame, S. J., and Balogh, A. (1994). Ulysses field and plasma observations of magnetic holes in the solar wind and their relation to mirror-mode structures. *Journal of Geophysical Research: Space Physics*, 99(A12):23371–23381.

Xiao, T., Shi, Q. Q., Tian, A. M., Sun, W. J., Zhang, H., Shen, X. C., Shang, W. S., and Du, A. M. (2014). Plasma and Magnetic-Field Characteristics of Magnetic Decreases in the Solar Wind at 1 AU: Cluster-C1 Observations. *Solar Physics*, 289(8):3175–3195.

Xiao, T., Shi, Q. Q., Zhang, T. L., Fu, S. Y., Li, L., Zong, Q. G., Pu, Z. Y., Xie, L., Sun, W. J., Liu, Z. X., Lucek, E., and Reme, H. (2010). Cluster-C1 observations on the geometrical structure of linear magnetic holes in the solar wind at 1 AU. *Annales Geophysicae*, 28(9):1695–1702.

Yao, S. T., Li, J. H., Zhou, X., Shi, Q. Q., Zong, Q., Zhang, H., Li, W. Y., Hamrin, M., Volwerk, M., Pitkänen, T., and Yang, F. (2023). Ion-Vortex Magnetic Hole With Reversed Field Direction in Earth's Magnetosheath. *Journal of Geophysical Research: Space Physics*, 128(7):e2023JA031749.

Yu, L., Huang, S. Y., Yuan, Z. G., Jiang, K., Xiong, Q. Y., Xu, S. B., Wei, Y. Y., Zhang, J., and Zhang, Z. H. (2021). Characteristics of Magnetic Holes in the Solar Wind Revealed by Parker Solar Probe. *The Astrophysical Journal*, 908(1):56.

Zhang, T. L., Russell, C. T., Baumjohann, W., Jian, L. K., Balikhin, M. A., Cao, J. B., Wang, C., Blanco-Cano, X., Glassmeier, K., Zambelli, W., Volwerk, M., Delva, M., and Vörös, Z. (2008a). Characteristic size and shape of the mirror mode structures in the solar wind at 0.72 AU. *Geophysical Research Letters*, 35(10):2008GL033793.

Zhang, T. L., Russell, C. T., Zambelli, W., Vörös, Z., Wang, C., Cao, J. B., Jian, L. K., Strangeway, R. J., Balikhin, M., Baumjohann, W., Delva, M., Volwerk, M., and Glassmeier, K. (2008b). Behavior of current sheets at directional magnetic discontinuities in the solar wind at 0.72 AU. *Geophysical Research Letters*, 35(24):2008GL036120.

Zurbuchen, T. H., Hefti, S., Fisk, L. A., Gloeckler, G., Schwadron, N. A., Smith, C. W., Ness, N. F., Skoug, R. M., McComas, D. J., and Burlaga, L. F. (2001). On the origin of microscale magnetic holes in the solar wind. *Journal of Geophysical Research: Space Physics*, 106(A8):16001–16010.